Brain variability in dynamic resting-state networks identified by fuzzy entropy: a scalp EEG study

Abstract

Objective. Exploring the temporal variability in spatial topology during the resting state attracts growing interest and becomes increasingly useful to tackle the cognitive process of brain networks. In particular, the temporal brain dynamics during the resting state may be delineated and quantified aligning with cognitive performance, but few studies investigated the temporal variability in the electroencephalogram (EEG) network as well as its relationship with cognitive performance. *Approach.* In this study, we proposed an EEG-based protocol to measure the nonlinear complexity of the dynamic resting-state network by applying the fuzzy entropy. To further validate its applicability, the fuzzy entropy was applied into simulated and two independent datasets (i.e., decision-making and P300). *Main results.* The simulation study first proved that compared to the existing methods, this approach could not only exactly capture the pattern dynamics in time series but also overcame the magnitude effect of time series. Concerning the two EEG datasets, the flexible and robust network architectures of the brain cortex at rest were identified and distributed at the bilateral temporal lobe and frontal/occipital lobe, respectively, whose variability metrics were found to accurately classify different groups. Moreover, ~~And~~ the temporal variability of resting-state network property was also either positively or negatively related to individual cognitive performance. *Significance.* This outcome suggested the potential of fuzzy entropy for evaluating the temporal variability of the dynamic resting-state brain networks, and the fuzzy entropy is also helpful for uncovering the fluctuating network variability that accounts for the individual decision differences.

Keywords: Fuzzy entropy, Resting-state EEG, Network variability, Decision-making

1. Introduction

Electroencephalogram (EEG) directly reflecting the neural electrical activity, is dynamic and varies across time scales. As one of the most complex dynamic systems, the brain constantly constructs and updates the internal network models to anticipate and plan future adaptive behaviors (Braun *et al* 2015, Jiang *et al* 2019). The brain at rest is also active both physiologically and psychologically (Damoiseaux *et al* 2006, Mantini *et al* 2007), and related resting-state brain activity has been proved to serve as the neural basis underlying the potential task information processing (Wang *et al* 2019, Hearne *et al* 2017). Just as illustrated, related brain networks at rest can effectively characterize the intrinsic allocation of the brain resources (Falahpour *et al* 2018, Northoff *et al* 2010) and also help predict the individual performance during the following tasks (Li *et al* 2013a, Zhou *et al* 2012) , as well as individual mental state (Tian *et al* 2017a). For example, both the resting-state network topologies and properties were found to be positively related to the P300 amplitudes that were evoked by the target stimuli during the oddball tasks (Li *et al* 2015). ~~and related network at rest can effectively characterize the intrinsic allocation of brain resources (Falahpour *et al* 2018, Li *et al* 2019b, Northoff *et al* 2010), and also helps to predict the individual task performance (Si *et al* 2019a, Zhang *et al* 2015, Li *et al* 2013a).~~ At its initial stage, the resting-state network is believed to be stable, while plenty of recent studies find that the brain network at rest also fluctuates over time (Betzel *et al* 2016, Yu *et al* 2015, Garrett *et al* 2011). To quantitatively capture the fluctuating brain variability, the sliding window is usually used, which measures the time series of the dynamic functional connectivity. Several methods are then developed to explore the fluctuating variability across the time scales, which includes the variance of dynamic network connectivity, the network dissimilarity over time, and non-linear test statistics (Sun *et al* 2019, Zalesky *et al* 2014, Sakoglu *et al* 2010). For example, the network dissimilarity illustrated that better individual verbal creativity correlates with higher temporal variability in resting-state functional connectivity among multiple regions, such as the lateral prefrontal cortex, parahippocampal gyrus, and precuneus (Sun *et al* 2019).

Theoretically, the more diverse the fluctuating patterns of a given time series are, the high complexity the corresponding time series will be, that is, the signal is more irregular. The temporal complexity of a system can index its fluctuating dynamics; for a given signal, entropy has been widely used to quantify the corresponding signal complexity. The entropy can nonlinearly measure how complex (i.e., level of irregularity) the physiological signal will be (Gao *et al* 2015) and thus is proportional to signal irregularity; the larger the entropy, the more irregular the signal. Therefore, measuring the signal entropy in the temporal domain will deepen our knowledge of brain dynamics (Abasolo *et al* 2006, Tian *et al* 2019, Tian *et al* 2017b) and provide the possibility to quantitatively evaluate the temporal complexity of the physiological system (Takahashi *et al* 2010). Fuzziness is an alternative approach used when describing the uncertainty of a time series and the corresponding fuzzy entropy measurement has been proved to have great potential for avoiding the undesirable boundary effect (a sharp distinction of the boundary), compared to the other entropies, such as approximate entropy and sample entropy (Chen *et al* 2009); in the meantime, stronger relative consistency and less dependence on data length of the Fuzzy entropy further facilitate its application in evaluating the signal complexity (Li *et al* 2013b, Xie *et al* 2010). Therefore, ~~can avoid the undesirable boundary effect (i.e., a sharp distinction of the boundary) (Rudas and Kaynak 1998); thus,~~ the

fuzzy entropy can effectively guarantee the estimated signal metrics to vary smoothly and continuously with similarity tolerance. Recently, fuzzy entropy has been widely applied to measure the complexity of both EEG and electromyogram (Cao *et al* 2018, Cao and Lin 2018, Masulli *et al* 2020), as well as investigating brain diseases, such as epileptic seizure (Cao *et al* 2020, Xiang *et al* 2015), schizophrenia (Yang *et al* 2015), and Alzheimer's Disease (AD) (Simons *et al* 2018). For example, when using the network-based Takagi-Sugeno-Kanga fuzzy classifiers to identify the AD patients, related network metrics under eyes-closed and eyes-open conditions achieved relatively high accuracies of 97.3% and 94.78%, respectively (Yu *et al* 2020).

However, most of the current approaches mainly focus on the amplitude stationarity of brain networks to measure the dynamics of the temporal network variability (Zalesky *et al* 2014, Hindriks *et al* 2016) but neglect the inherent fluctuating network patterns that are remarkably helpful for reflecting how the brain network fluctuates over time. As illustrated previously, the corresponding network patterns, such as the network topological alterations, could promote the classification among different conditions (Moon *et al* 2020, Pena-Gomez *et al* 2018). For example, Shirer and colleagues used the whole-brain connectivity patterns to decode subject-driven cognitive states and achieved an accuracy of 84% (Shirer *et al* 2012), and when using network topological alterations to accomplish the fatigue classification, Dimitrakopoulos and colleagues also achieve high accuracy of 92% for driving and 97% for psychomotor vigilance task (Dimitrakopoulos *et al* 2018).~~However, most of the current approaches mainly focus on the amplitude stationarity of brain networks to measure the dynamics of temporal variability in brain networks but neglect the inherent fluctuating patterns of networks that seem to be more important to reflect how the brain network fluctuates over time.~~ Moreover, corresponding network complexity has also been proved to have great potential for indexing the flexible and robust network architectures and reflecting how the brain could respond to cognitive stimuli (Sun *et al* 2019). To effectively explore the mechanism underlying the cognitive process in the brain, exactly capturing the fluctuating network patterns, e.g., flexible and robust architectures, will play an important role and help reflect to which degree the brain can respond to the upcoming task. Therefore, contrary to the traditional methods that measure the amplitude stationarity (Zalesky *et al* 2014, Hindriks *et al* 2016), our current work mainly focused on exploring the fluctuating temporal patterns of the time-varying resting-state brain networks, to uncover the potential fuzzy evidence underlying the decision differences between different individuals.~~When exploring the neural mechanism underlying the cognitive process, exactly and effectively capturing the fluctuating network patterns, e.g., flexible and robust architectures, will be more crucial, and helps reflect to which degree the brain could respond to the upcoming task from the perspective of the brain networks. Therefore, contrary to traditional approaches that measure the amplitude stationarity, our current work mainly focused on investigating the fluctuating temporal patterns of resting-state brain networks over time. And the corresponding flexible and robust architectures would be then effectively captured by the fuzzy entropy, whose variability metrics could accurately reflect how the brain network architecture fluctuates over time.~~

Herein, we assumed that the fluctuating temporal variability in resting-state networks can be effectively captured by fuzzy entropy, and related variability metrics do closely relate to individual cognitive behaviors. To validate this approach, besides a simulation study, the

proposed metric was further applied to the real dataset of decision-making that was collected from adolescents and adults when they responded to the unfair offers. As a high-level cognitive process, decision-making involves a wide range of complex behaviors (Cecchetto *et al* 2017, Preuss *et al* 2016) and is attributed to the functional interactions of those spatially separated but functionally linked brain regions (Si *et al* 2020a, Si *et al* 2019b). Understanding the neural substrates of decision-making helps establish effective artificial intelligence and brain-computer interface (BCI) as well, where the decision-making is of great importance for individuals (Long *et al* 2012, Li *et al* 2013c). The theories of (culture-specific) socialization (Hoffmann and Tee 2006, Marchetti *et al* 2019) and childhood development (Castelli *et al* 2010, Castelli *et al* 2014, Guroglu *et al* 2009) demonstrate that the preference for fairness increases with age, and adolescents usually make relatively larger acceptances than the adults, as they preferred the outcome even under unfair conditions (Sutter 2007, Si *et al* 2020b).

Moreover, P300 has also been demonstrated to be attributed to the functional interactions of multiple regions in the brain, including the middle frontal gyrus, insula, and thalamus, etc (Li *et al* 2020, Bledowski *et al* 2004), and could effectively index various cognitive functions, such as attention allocations and working memory (Polich 2007). As one of the electrophysiological biomarkers, P300 has been widely used to evaluate the subject's capacity during tasks (Wang *et al* 2015a), as well as classify different individual groups (Turetsky *et al* 2015). Uncovering related neural mechanism also helps deepen our understanding of P300 and contributes to its future applications in multiple aspects, such as BCI and clinical diseases, etc. Following decision-making, to further validate the applicability of the fuzzy entropy in capturing the fluctuating temporal variability of resting-state networks, an independent P300 resting-state EEG dataset was also investigated by adopting the same analytical protocols.

2. Materials and methods

2.1. *Fuzzy entropy of the dynamic networks*

Fuzzy entropy can effectively evaluate signal complexity, especially for the short time series contaminated by noise (Chen et al 2009), and is insensitive to disturbance but sensitive to the fluctuations of related information content (Acharya et al 2015). A higher value of fuzzy entropy represents the larger temporal variability in time series.

Assuming there are N networks, the time series for each network edge can be termed as X_i ($1 \le i \le N$) whose value varies from 0 to 1, which is formed as follows;

$$X_i^m = \{u(i), u(i+1), \ldots, u(i+m-1)\} - u_0(i), i = 1, \ldots, N-m+1 \quad (1)$$

where X_i^m represents m consecutive u values (i.e., coherence value) at i-th network point, which is generalized by removing the baseline $u_0(i) = m^{-1}\sum_{j=0}^{m-1} n(i+j)$.

Given r, calculating the similarity degree D_{ij}^m between X_i^m and its neighboring vector X_j^m, which is formulized as follow;

$$D_{ij}^m = \mu(d_{ij}^m, r) \quad (2)$$

where d_{ij}^m is the maximum absolute difference of the corresponding scalar components of X_i^m and X_j^m. For each vector X_i^m (i = 1, 2, …, N-m+1), by averaging all similarity degree, D_{ij}^m, of

its neighboring vectors X_j^m (i = 1, 2, …, N-m+1, and $j \neq i$), we then get

$$\phi_i^m(r) = (N-m-1)^{-1} \sum_{j=1, j\neq i}^{N-m} D_{ij}^m \quad (3)$$

Relying on $\varphi^m(r) = (N-m)^{-1} \sum_{i=1}^{N-m} \phi_i^m(r)$ and $\varphi^{m+1}(r) = (N-m)^{-1} \sum_{i=1}^{N-m} \phi_i^{m+1}(r)$, we then define the *FuzzEn*(m, r) of the time series X_i ($1 \leq i \leq N$) as follow;

$$FuzzEn(m,r) = \lim_{N\to\infty} \left[\ln \varphi^m(r) - \ln \varphi^{m+1}(r)\right] \quad (4)$$

which can be estimated by the statistic,

$$FuzzEn(m,r,N) = \ln \varphi^m(r) - \ln \varphi^{m+1}(r) \quad (5)$$

where m denotes the length of the compared window, r denotes the width of the boundary for similarity measurement, and N denotes the length of related time series to be analyzed. Particularly, large m guarantees a more detailed reconstruction of the dynamic process, but an overlarge m might lead to information loss (Pincus and Goldberger 1994). Just as proposed in the previous study (Chen *et al* 2007), m was determined to be 2. In the meantime, rather small r brings the noise, but too large r might also result in information loss, which is, therefore, set to 0.2 multiplied by the standard deviation of the time series in this study.

2.2. *Validation on simulated data*

To evaluate whether the proposed fuzzy entropy-based analysis could capture the fluctuating temporal variability in the dynamic resting-state networks, we first simulated the dynamic networks that varied across time scales, whose network edge strengths vary over time. To fulfill this aim, the *MIX*(p) with varying parameter p values ($0 \leq p \leq 1$) was used to formulate the network edges between two nodes (Pincus 1991, Pincus 1995), whose time series had varying complexity. The *MIX*(p) is a series of sampling processes for the stacking waves of sines and cosines at p = 0 or independent uniform random variables at p = 1. Meanwhile, to test if the proposed method was sensitive to the magnitude of the signal, the varying magnitudes were also simulated with another parameter i, as i was set as 0.1, 0.5, 1, 5, and 10. Herein, for each time point j in the simulated time series, we first defined the $MIX^{(i)}(p)$ as follow;

$$MIX^{(i)}(p)_j = i(1-Z_j)X_j + Z_jY_j - H_j \quad (6)$$

where X_j represents the stochastic and deterministic signal formed by the sine and cosine signal, and $X_j = \frac{7}{100}\times\sin\left(\frac{\pi}{50}\times j+\frac{\pi}{6}\right)+\frac{3}{100}\times\sin\left(\frac{\pi}{500}\times j+\frac{\pi}{6}\right)+\frac{1}{25}\times\cos\left(\frac{9\pi}{1000}\times j\right)+\frac{1}{20}\times\cos\left(\frac{\pi}{125}\times j\right)+0.8$, Y_j represents a family of independent identically distributed real random variables, with uniform density in the interval [0, 0.3], Z_j represents the random variable, where Z_j = 1 with probability p, Z_j = 0 with probability 1 - p, and H_j represents a discrete step function.

As the p-value increases, the time process becomes intuitively more irregular, that is, a larger p denotes the higher complexity of the signal (i.e., the corresponding edge has more complicated patterns). In this study, we simulated a weighted network with 5 nodes (Fig. 3a), in which each edge had varied predefined complexity with the p-value being selected within a

range of [0.1, 0.5]. With the predefined signal complexity determined by p, the five time-varying edges were simulated between pairs of nodes (nodes A and C, nodes B and D, nodes C and D, nodes C and E, and nodes D and E) in Fig. 3a.

In this study, apart from the fuzzy entropy, other traditional approaches, such as variance (Sakoglu *et al* 2010) and non-linear test statistic (Zalesky *et al* 2014), were also used to measure related fluctuating temporal complexity of these edges in our predefined 5-nodes network. Furthermore, to acquire a robust simulated result, the $MIX^{(i)}(p)$ and the estimation of fluctuating temporal complexity were repeated 1,000 times. Finally, the averaging across 1000 times is used to evaluate and compare the capacity of different approaches in measuring the fluctuating temporal variability of the brain networks.

2.3. *Validation on decision-making data*

2.3.1. Participants. The experiment protocol was approved by the Institution Research Ethics Board of XXX and was conducted following the Declaration of Helsinki. Two independent groups of participants (i.e., postgraduate and junior high school students) were recruited and paid for their efforts to take part in this study at XXX. Before they joined our experiments, participants were told about the experimental details and then read and signed their names on the written informed consent. Eighteen postgraduate students (5 females, age range of 21-24 years, and mean 23.45 years) from the XXX and 22 junior high school students (10 females, age range of 14-16 years, and mean 14.59 years) from XXX were included in this study. None of the participants had a history of neurological or psychiatric disorders and were not currently using any psychoactive medications. All of them had normal or correct-to-normal visual acuity.~~The experiment protocol was approved by the Institution Research Ethics Board of the University of Electronic Science and Technology of China (UESTC) and was conducted in accordance with the Declaration of Helsinki. Two independent groups of participants (i.e., postgraduate and junior high school students) were recruited and paid for their efforts to take part in this study at UESTC. Before they joined our experiments, participants were told about the experimental details and then read and signed their name on the written informed consent. Eighteen postgraduate students (5 females, age range of 21-24 years, and mean 23.45 years) from the UESTC and 22 junior high school students (10 females, age range of 14-16 years, and mean 14.59 years) from The Experimental High School Attached To UESTC were included in this study. None of the participants had a history of neurological or psychiatric disorders and were not currently using any psychoactive medications; meanwhile, all of them had normal or correct-to-normal visual acuity.~~

2.3.2. Experimental protocols. In the ultimatum game (UG) task, the participant acted as a responder who would decide to accept or reject an offer given by the proposer (i.e., the computer itself). If he or she accepted the offer, both players (i.e., responder and proposer) received the money according to the splits; in case of rejecting it, they would not earn anything. When playing with the computer game, participants were advised to play this game with another participant in a separate room. Experiments were performed in a quiet, dimly lightroom. Participants were first instructed to take a deep breath to adapt to the experimental environment. Before the UG task, 5 minutes of eyes-closed resting-state EEG datasets were recorded, which was followed by an 8.5 min UG task.

~~2.3.2. In the ultimatum game (UG) task, the participant acted as a responder who would decide to accept or reject an offer given by the proposer (i.e., the computer itself). If he or she accepted the offer, both players (i.e., responder and proposer) received the money according to the splits; in case of rejecting it, they would not earn anything. When playing with the computer game, participants were advised to play this game with another participant in a separate room. Experiments were performed in a quiet, dimly lightroom. Participants were first instructed to take a deep breath to adapt to the experimental environment. Before the UG task, 5 minutes of eyes-closed resting-state EEG datasets were recorded, which was followed by an 8.5 min UG task.~~

Fig. 1 illustrates the timeline of the UG task. In the UG task, the sum of splits was ¥ 10; meanwhile, three categories were included, i.e., the fair offer (¥ 5 vs. ¥ 5), moderately unfair offer (¥ 3 vs. ¥ 7), and extremely unfair offer (¥ 1 vs. ¥ 9). A total of 90 offers, 30 offers per condition, were included in the UG task. Each UG trial began with an 800 ms thin cross. Then, a screen with ¥ 10 appeared and lasted 500 ms, which was followed by a 1,000 ms black screen. Thereafter, a split offer was presented, at the same time, participants need to decide to reject ("3") or accept ("1") the offer by pressing the button on the standard keyboard. Followed by their choice, the feedback appeared to inform their received money on that trial, as well as the cumulative winnings of participants. The decision and feedback would keep 2,700 ms in total.

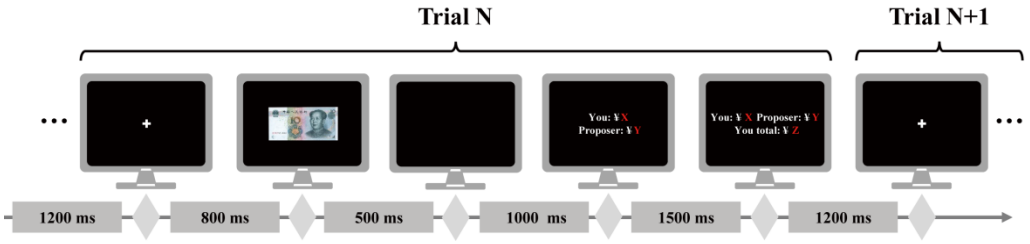

Fig. 1. The timeline of a UG task trial.

2.3.3. EEG recording. Participants were seated in an electrically shielded and light-attenuated room. The 64-channels resting-state EEG datasets were recorded by using the ASA-Lab Amplifier (ANT Neuro), and the 64 Ag/AgCl electrodes were positioned in compliance with the extended 10-20 international electrode system. During the data recording, the EEGs were digitized with a sampling rate of 500 Hz, and online bandpass filtered within the frequency range of [0.05 Hz, 70 Hz]. The electrodes of CPz and AFz served as the reference and ground, respectively. The electrooculogram was recorded from one channel located at the above side of the left eye to monitor eye movements. For all electrodes, the impedance was consistently below 5 KΩ throughout the experiment~~Participants were seated in an electrically shielded and light-attenuated room. The 64-channels resting-state EEG datasets were recorded by using the ASA-Lab Amplifier (ANT Neuro), and the 64 Ag/AgCl electrodes were positioned in compliance with the extended 10-20 international electrode system. During the data recording, the EEGs were digitized with a sampling rate of 500 Hz, and online bandpass filtered within the frequency range of [0.05 Hz, 70 Hz]. The electrodes of CPz and AFz served as the reference and ground, respectively. The electrooculogram was recorded from one channel located at the above side of the left eye to monitor eye movements. For all electrodes, the impedance was consistently below 5 KΩ throughout the experiment.~~

2.3.4. ~~EEG processing~~Fuzzy entropy of resting-state EEG network. In fact, these decision-making datasets had been reported in our previous study (Si *et al* 2019b), since our present study focused on investigating the resting-state network variability, only the resting-state EEG datasets were used here. Although the potential mechanism of the decision-making differences had been explored in previous studies from the perspective of ERP and power spectra, etc (Villafaina et al 2019, Kim et al 2021), decision-making is proved to be attributed to the functional interactions of those spatially separated but functionally coupled regions (Si et al 2020a, Si et al 2019b). Moreover, related fluctuating temporal patterns in decision networks are still been left unveiled, although the corresponding network complexity has also been proved to help identify the temporal variability in network architecture and index how the brain responds to cognitive stimuli (Sun *et al* 2019, Zalesky *et al* 2014). Therefore, when exploring the potential mechanism underlying the decision-making, identifying the corresponding temporal variability in decision network architectures, e.g., flexible and robust network patterns, will be of great importance and also help index to which degree the brain could respond to the unfair conditions. The analytical protocols for exploring the brain variability in dynamic resting-state networks were first displayed in Fig. 2, and the detailed procedures were further depicted as follows.

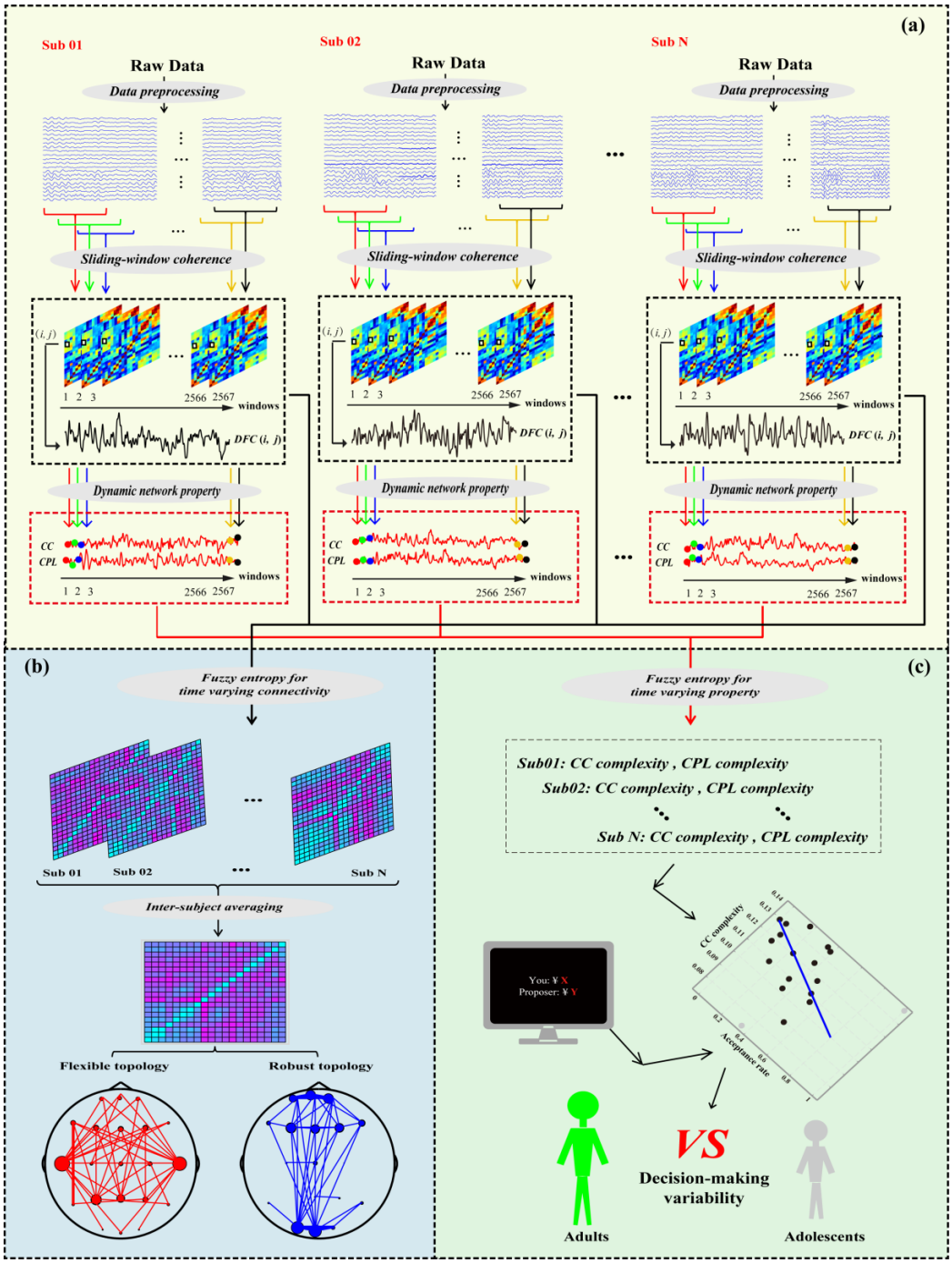

Fig. 2. Analytical protocols of the temporal variability in the resting-state EEG network. (a) Dynamic resting-state network construction, (b) The complexity of the dynamic resting-state network topologies, and (c) The temporal complexity of the dynamic resting-state network properties and Pearson's correlation analysis between network properties complexity and UG task behaviors. DFC denotes dynamic functional connectivity.

Before exploring related brain variability in these time-varying resting-state networks, the resting-state EEG datasets were first preprocessed. Concretely, to remove the artifacts, the resting-state EEG datasets were first referenced to a neutral reference of Reference Electrode Standardization Technique (REST) (Dong *et al* 2017, Yao 2001), and then offline bandpass

filtered within the frequency range of [0.5 Hz, 30 Hz]. Thereafter, the independent component analysis (ICA) was adopted to remove residual artifacts (He *et al* 2005) that still contaminate EEG data by removing related artifact components.

~~*Resting-state EEG network.*~~ The brain network is typically modeled by graph theory and includes a collection of nodes and edges. The EEG electrodes were considered as network nodes, and the synchronized strengths between pairwise electrodes estimated by coherence were set as network edges. Due to the effect of volume conduction, the nearby electrodes acquire similar contributions from cortical sources and thus capture a similar activity. In our present study, to reduce the effect of volume conduction, following the procedure in related studies (Qin *et al* 2010, Huang *et al* 2017), 21 canonical electrodes (i.e., FP1/z/2, F7/3/z/4/8, T7/8, C3/z/4, P7/3/z/4/8, and O1/z/2) out of the 64 channels in the 10-20 system were used to construct the resting-state network. Theoretically, coherence can effectively measure the synchronized neuronal assembly at any given frequency bin f between pairwise signals, $x(t)$ and $y(t)$, and is usually formulated as,

$$C_{xy}(f) = \left|R_{xy}(f)\right|^2 = \frac{\left|P_{xy}(f)\right|^2}{P_{xx}(f)P_{yy}(f)} \quad (1)$$

where $C_{xy}(f)$ and $R_{xy}(f)$ represent the estimated coherence value and the complex correlation coefficient between $x(t)$ and $y(t)$ at frequency bin f, respectively. At per frequency bin f, $P_{xy}(f)$ represents the cross-spectrum between $x(t)$ and $y(t)$, $P_{xx}(f)$ and $P_{yy}(f)$ represent the auto-spectrum of $x(t)$ and $y(t)$, respectively. These measurements of spectral densities were calculated from the Fast Fourier Transform. For each frequency bin f, the $C_{xy}(f)$ is calculated by squaring the magnitude of the complex correlation coefficient R between $x(t)$ and $y(t)$, which returns a real value within the range of [0, 1]. Since this study focused on the fluctuating variability of brain activity at rest, we thus concentrated on the alpha band ([8, 13] Hz) to construct the corresponding resting-state network.

In our present study, the time-resolved resting-state network was calculated by using a 5-s sliding-window approach with an overlapping of 98% that can provide ~~the~~ 100 ms temporal resolution for dynamic networks, which resulted in the time-varying networks varied across time scales. ~~, whose protocols were further depicted in Fig. 2.~~

~~The network is constructed based on each 5-s segment with 98% overlapping, resulting in the dynamic networks varied across time scales.~~ Based on the time-varying ~~dynamic~~ resting-state networks, a time series would be obtained for each network edge, and when the corresponding variability is calculated for each edge by the fuzzy entropy, the variability of network topology could be achieved, which can reflect how stable each network edge is (Fig. 2a). After the above procedure, each subject will have a network topology complexity and a network property complexity. For network topological complexity, it can reveal the distribution of spatial topological variability clearly, which can reflect the robust or flexible spatial pattern. Finally, by grand-averaging across subjects, the network topology complexity accounting for all subjects could be achieved (Fig. 2b).

~~Meanwhile, by using the brain connectivity toolbox (BCT), we quantitatively calculated the corresponding network properties for each dynamic network, resulting in the dynamic resting-state network properties (i.e., *CC*, *CPL*, *GE*, *LE*, and small-worldness) that varied~~

across time. Then, the temporal variability of these parameters could also be quantitatively measured by the fuzzy entropy, which reflected the fluctuating complexity in the properties time series (Fig. 2a).

Thereafter, a threshold strategy was used in identifying the fluctuating temporal patterns in resting-state networks; concretely, the 20% network edges with the largest and smallest fuzzy entropy were adopted to index the flexible and robust network architectures for both groups, respectively. However, when calculating related resting-state network properties,

Fuzzy entropy. Fuzzy entropy can effectively evaluate signal complexity, especially for the short time series contaminated by noise (Chen *et al* 2009), and is insensitive to disturbance and sensitive to the change of information content (Acharya *et al* 2015). A higher value of fuzzy entropy represents the larger temporal variability in time series.

Assuming there are N networks, the time series for each network edge can be termed as X_i $(1 \le i \le N)$ whose value varies from 0 to 1, which is formed as follows;

$$X_i^m = \{u(i), u(i+1), \ldots, u(i+m-1)\} - u0(i), i = 1, \ldots, N-m+1 \quad (2)$$

where X_i^m represents m consecutive u values (i.e., coherence value) at i-th network point, which is generalized by removing the baseline $u0(i) = m^{-1}\sum_{j=0}^{m-1} u(i+j)$.

Given r, calculating the similarity degree D_{ij}^m between X_i^m and its neighboring vector X_j^m, which is formulized as follow;

$$D_{ij}^m = \mu\left(d_{ij}^m, r\right) \quad (3)$$

where d_{ij}^m is the maximum absolute difference of the corresponding scalar components of X_i^m and X_j^m. For each vector X_i^m $(i = 1, 2, \ldots, N-m+1)$, by averaging all similarity degree, D_{ij}^m, of its neighboring vectors X_j^m $(i = 1, 2, \ldots, N-m+1$, and $j \ne i)$, we then get

$$\phi_i^m(r) = (N-m-1)^{-1}\sum_{j=1, j\ne i}^{N-m} D_{ij}^m \quad (4)$$

Relying on $\varphi^m(r) = (N-m)^{-1}\sum_{i=1}^{N-m}\phi_i^m(r)$ and $\varphi^{m+1}(r) = (N-m)^{-1}\sum_{i=1}^{N-m}\phi_i^{m+1}(r)$, we then define the *FuzzEn*(m, r) of the time series X_i $(1 \le i \le N)$ as follow;

$$FuzzEn(m, r) = \lim_{N\to\infty}\left[\ln\varphi^m(r) - \ln\varphi^{m+1}(r)\right] \quad (5)$$

which can be estimated by the statistic,

$$FuzzEn(m, r, N) = \ln\varphi^m(r) - \ln\varphi^{m+1}(r) \quad (6)$$

In this definition, m denotes the embedded dimension and r denotes the fuzzy similarity boundary. Larger m means the more detailed reconstruction of the dynamic process, we then set m to 2. Rather small r might bring the noise, whereas too large r might lead to information loss (Chen *et al* 2007), which is, therefore, set to 0.2 multiplied by the standard deviation of the time series in this study.

Fuzzy entropy of network property. Multiple network properties, including nodal degree (*ND*), clustering coefficients (*CC*), global efficiency (*GE*), local efficiency (*LE*), and characteristic path length (*CPL*) (Rubinov and Sporns 2010), the fully-connected weighted adjacency matrices

without any thresholding were used. ~~can be used to quantitatively measure brain network [46].~~ Theoretically, the *ND* sums all edge strengths connecting one network node and reflects the importance of this node in a given network, the *CC* and *LE* index the functional segregation of a given network and both reflect the capacity for specialized processing within densely interconnected regions, while the *CPL* and *GE* measure the functional integration and index the ability to rapidly combine specialized information from distributed regions. Here, based on the fully-connected weighted adjacency matrix per subject, let C_{ij} be the synchronized strength between nodes i and j estimated by coherence, d_{ij} represents the shortest weighted path length, N represents the number of all nodes, and Θ represents the set of network nodes. The *ND*, *CC*, *GE*, *LE*, and *CPL* were then formulized as follows.

$$ND_i = \sum_{j\in\Theta} C_{ij} \quad (7\text{-}8)$$

$$CC = \frac{1}{N}\sum_{i\in\Theta}\frac{\sum_{j,l\in\Theta}\left(C_{ij}C_{il}C_{jl}\right)^{1/3}}{\sum_{j\in\Theta}C_{ij}\left(\sum_{j\in\Theta}C_{ij}-1\right)} \quad (8\text{-}9)$$

$$CPL = \frac{1}{N}\sum_{i\in\Theta}\frac{\sum_{j\in\Theta, j\neq i} d_{ij}}{N-1} \quad (9\text{-}10)$$

$$GE = \frac{1}{N}\sum_{i\in\Theta}\frac{\sum_{j\in\Psi, j\neq i}\left(d_{ij}\right)^{-1}}{N-1} \quad (10\text{-}11)$$

$$LE = \frac{1}{N}\sum_{i\in\Theta}\frac{\sum_{j,h\in\Theta, j\neq i}\left(w_{ij}w_{ih}\left[d_{jh}\left(\Theta_i\right)\right]^{-1}\right)^{1/3}}{\sum_{j\in\Theta}w_{ij}\left(\sum_{j\in\Theta}w_{ij}-1\right)} \quad (11\text{-}12)$$

Since the small-worldness has been widely used in brain networks to investigate the human cognitive process (Bassett and Bullmore 2017), as well as measuring the capacity of stimuli modulation, such as acupuncture (Yu *et al* 2018), in our present study, the small-worldness is also adopted as one of the variability metrics to measure the resting-state brain networks. Theoretically, small-worldness is quantified by the *CPL* and *CC* and reflects the regional specialization and the information transfer efficiency in the brain. Before calculating the small-worldness, the *CC* and *CPL* of the constructed EEG networks (i.e., CC_t and CPL_t) are normalized by dividing by the value for the same variable calculated for a randomly rewired null model, which are then termed as γ and λ, respectively. Here, the *CC* and *CPL* of the random network (i.e., CC_r and CPL_r) are the averages of the values calculated from 1000 randomly rewired null models.

$$\gamma = \frac{CC_t}{CC_r} \quad (12\text{-}13)$$

$$\lambda = \frac{CPL_t}{CPL_r} \quad (13\text{-}14)$$

Finally, the small-worldness, *sw*, is given by a ratio of the normalized *CC*, γ, to the normalized *CPL*, λ, as,

$$sw = \frac{\gamma}{\lambda} \quad (14\underline{15})$$

Herein, by using the brain connectivity toolbox (BCT), we quantitatively calculated the corresponding network properties for each dynamic network, resulting in the dynamic resting-state network properties (i.e., *CC*, *CPL*, *GE*, *LE*, and small-worldness) that varied across time. Then, the temporal variability of these parameters could also be quantitatively measured by the fuzzy entropy, which reflected the fluctuating complexity in the properties time series (Yu *et al* 2015, Thompson *et al* 2017) (Fig. 2a).

Although, the acceptance rate (AR) varies across subjects but relatively keeps stable intra-subject, and is thus used to characterize the individual task behavior during tasks (Wang *et al* 2017). Besides, the cumulative winning~~s~~ (CW) is also regarded as a direct measurement of task behavior during the UG task. We then obtained the AR of combining the extremely and moderately unfairness conditions, as well as the CW throughout the UG task.~~In this study, to investigate the underlying relationship between the resting-state network variability and individual task behaviors (Pedersen *et al* 2018), we then quantitatively obtained the AR of combining the extremely and moderately unfairness conditions, as well as the CW throughout the UG task.~~

~~In our study, the time-resolved resting-state network was calculated by using a 5-s sliding-window approach with overlapping of 98% that can provide the 100-ms temporal resolution for dynamic networks, whose protocols were further depicted in Fig. 2.~~

~~The network is constructed based on each 5-s segment with 98% overlapping, resulting in the dynamic networks varied across time scales. Based on the dynamic resting-state networks, a time series would be obtained for each network edge, and when the corresponding variability is calculated for each edge by the fuzzy entropy, the variability of network topology could be achieved, which can reflect how stable each network edge is (Fig. 2a). Meanwhile, by using the brain connectivity toolbox (BCT), we quantitatively calculated the corresponding network properties for each dynamic network, resulting in the dynamic resting-state network properties (i.e., *CC*, *CPL*, *GE*, *LE*, and small-worldness) that varied across time. Then, the temporal variability of these parameters could also be quantitatively measured by the fuzzy entropy, which reflected the fluctuating complexity in the properties time series (Yu *et al* 2015, Thompson *et al* 2017) (Fig. 2a).~~

~~After the above procedure, each subject will have a network topology complexity and a network property complexity. For network topology complexity, it can reveal the distribution of spatial topology variability clearly, which can reflect the stable or flexible spatial pattern. Finally, by grand-averaging across subjects, the network topology complexity accounting for all subjects could be achieved (Fig. 2b).~~ As proved in previous studies, the corresponding resting-state brain network has great potential for facilitating the prediction of individual performance during the following tasks (Li *et al* 2013a, Zhou *et al* 2012), for example, when using related resting-state network properties to predict individual acceptance rate during the UG task, the predicted rates were also found to be significantly correlated with the actual rates (Si *et al* 2019a). In our present study, concerning the resting-state network properties complexity, the correlation analysis was further implemented to investigate any possible relationships between resting-state network properties complexity and individual decision behavior (AR and CW, Fig. 2c). To obtain the robust representative knowledge underlying

the variability in decision-making between the two groups, the outliers were marked relying on the relationships between network property variability and task behaviors. In detail, participants with the 10% largest Malahanobis distances (Zhang *et al* 2015) to the data center were considered as the outliers and then excluded from the correlation analysis.

3. Results

3.1. Simulated network

To evaluate whether the proposed fuzzy entropy-based analysis could capture the fluctuating temporal variability in the dynamic resting-state networks, we first simulated the dynamic networks that varied across time scales, whose network edge strengths vary over time. To fulfill this aim, the $MIX(p)$ with varying parameter p values ($0 \leq p \leq 1$) was used to formulate the network edges between two nodes (Pincus 1991, Pincus 1995), whose time series had the varying complexity. The $MIX(p)$ is a series of sampling processes for the stacking waves of sines and cosines at $p = 0$ or independent uniform random variables at $p = 1$. Meanwhile, to test if the proposed method was sensitive to the magnitude of the signal, the varying magnitudes were also simulated with another parameter i, as i was set as 0.1, 0.5, 1, 5, and 10. Herein, for each time point j in the simulated time series, we first defined the $MIX^{(i)}(p)$ as follow;

$$MIX^{(i)}(p)_j = i(1 - Z_j)X_j + Z_j Y_j - H_j \quad (15)$$

where X_j represents the stochastic and deterministic signal formed by the sine and cosine signal, and $X_j = \frac{7}{100} \times \sin\left(\frac{\pi}{50} \times j + \frac{\pi}{6}\right) + \frac{3}{100} \times \sin\left(\frac{\pi}{500} \times j + \frac{\pi}{6}\right) + \frac{1}{25} \times \cos\left(\frac{9\pi}{1000} \times j\right) + \frac{1}{20} \times \cos\left(\frac{\pi}{125} \times j\right) + 0.8$, Y_j represents a family of independent identically distributed real random variables, with uniform density in the interval [0, 0.3], Z_j represents the random variable, where $Z_j = 1$ with probability p, $Z_j = 0$ with probability $1 - p$, and H_j represents a discrete step function.

As the p value increases, the time process becomes intuitively more irregular, that is, a larger p denotes the higher complexity of the signal (i.e., the corresponding edge has more complicated patterns). In this study, we simulated a weighted network with 5 nodes (Fig. 3a), in which each edge had varied predefined complexity with the p value being selected within a range of [0.1, 0.5]. With the predefined signal complexity determined by p, the five time-varying edges were simulated between pairs of nodes (nodes A and C, nodes B and D, nodes C and D, nodes C and E, and nodes D and E) in Fig. 3a.

In this study, apart from the fuzzy entropy, other approaches such as variance (Sakoglu *et al* 2010) and non-linear test statistic (Zalesky *et al* 2014) were also used to measure the corresponding temporal fluctuating complexity of these edges in our predefined 5-nodes network. Furthermore, to acquire a robust simulated result, the $MIX^{(i)}(p)$ and the estimation of temporal fluctuating complexity were repeated 1,000 times. Finally, the averaging across 1000 times is used to evaluate and compare the capacity of different approaches in measuring the fluctuating temporal variability of the brain networks.

In this simulation study, the complexity of each network edge measured by the fuzzy entropy was first displayed in Fig. 3b, which The complexity of each network edge measured by the

~~fuzzy entropy (Fig. 3b)~~ demonstrated a similar tendency with the predefined complexity per time series (Fig. 3a), for example, the edge D-E showed the largest complexity in both Fig. 3a and 3b. However, as shown in Figs. 3c and 3d, the other two methods inversely presented the largest complexity of edge A-C that had the smallest complexity in the current simulation, which unfortunately estimated the opposite tendency of the temporal complexity.

Moreover, the variance and non-linear test statistic were found to be indeed sensitive to the magnitude of the signal. Along with the increased magnitude, both methods estimated the increased signal complexity, which revealed $MIX^{(10)}(p) > MIX^{(5)}(p) > MIX^{(1)}(p) > MIX^{(0.5)}(p) > MIX^{(0.1)}(p)$ per complexity case (Fig. 3f and 3g). In contrast, the fuzzy entropy was not affected by the increased magnitude (Fig. 3e), as the same complexity was accurately estimated by the fuzzy entropy for all the five magnitude cases.

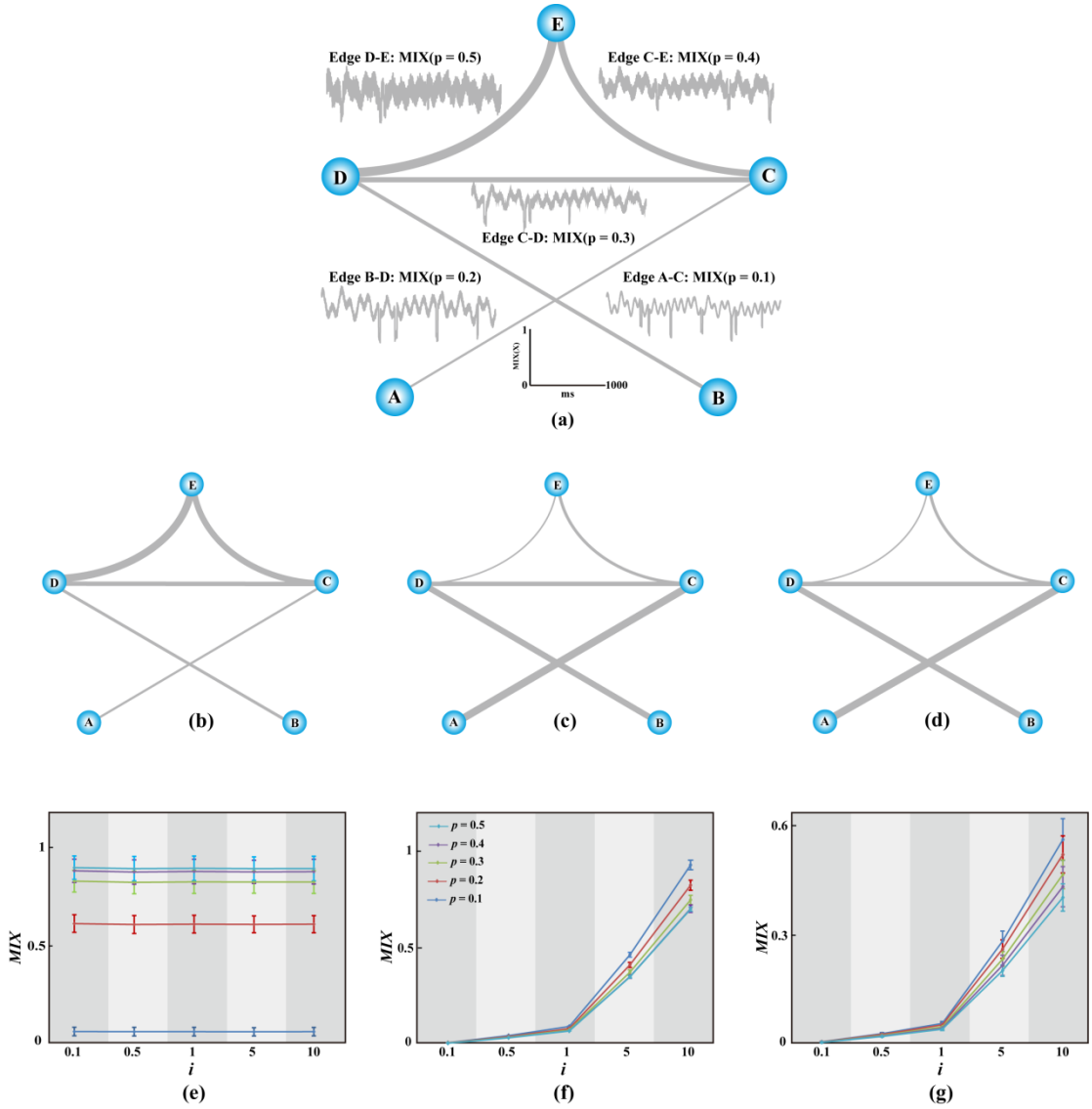

Fig. 3. Simulated 5-nodes network with $MIX^{(i)}(p)$ (p = 0.1, 0.2, 0.3, 0.4, and 0.5) (a) and the estimated temporal complexity of the network edge by the fuzzy entropy (b), variance (c), and non-linear test statistic (d). In subfigures (b - d), the width of the solid line denotes the predefined or estimated temporal complexity of a given edge. Subfigures (e - g) denote the varied temporal complexity of the network edge estimated by the fuzzy entropy (e), variance

(f), and non-linear test statistic (g) for all the five magnitude cases.

3.2. Variability in decision-making network topology

Figs. 4a and 4b display the 20% network edges with the largest (i.e., flexible) and smallest (i.e., robust) fuzzy entropy, respectively. Specifically, the flexible architectures of both postgraduate and junior high school students were consistently distributed at the bilateral temporal lobe (Fig. 4a), and the nodes were further printed with deep red color (i.e., high entropy) as shown in Fig. 4c. By contrast, for both groups, Fig. 4b illustrates a similarly robust architecture that seemed to be a resting-state default mode network (DMN), where the 20% edges with the smallest fuzzy entropy linked the frontal and occipital lobe.

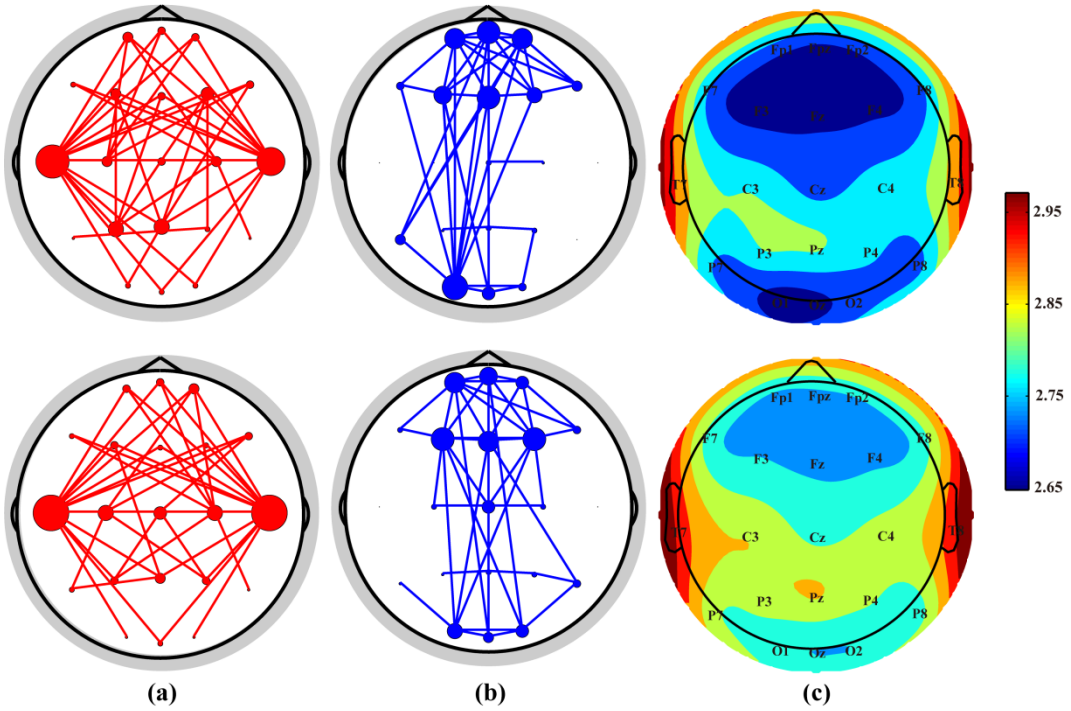

Fig. 4. Scalp topologies with the 20% largest and smallest fuzzy entropy for both groups. (a) Flexible architecture, (b) Robust architecture, and (c) Nodal degree ~~ND~~ distribution. The first and second row denotes the postgraduate students and junior high school students, respectively. In subfigures (a, b), the size of each electrode is proportional to its binary degree in the 20% largest and smallest network, respectively.

3.3. The relationships between network variability and decision behaviors

Thereafter, for both flexible and robust resting-state network architectures displayed in Fig. 4, the weights of flexible and robust network edges were averaged separately to achieve the averaged flexible and robust variability metrics per student in both postgraduates and junior high school groups. Thereafter, the averaged flexible and robust variability metrics of both groups were statistically compared separately, and as displayed in Fig. 5, we found the flexible metrics of postgraduate students were significantly larger than that of junior high school students (p ~~=~~ < 0.~~0~~0005), while the robust metrics between two groups were opposite to the flexible metrics (p <= 0.0~~0~~5).

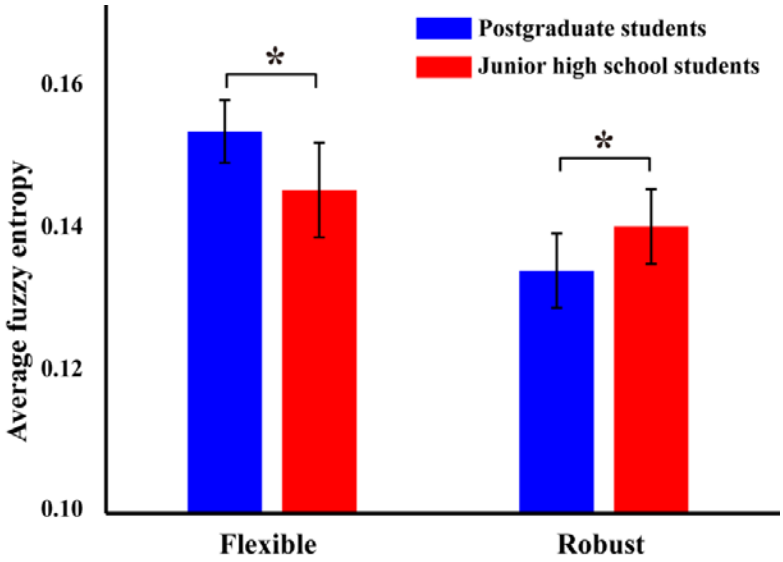

Fig. 5. The differences in the flexible and robust network variability metrics between postgraduate students and junior high school students. The red-filled bars denote the junior high school students, the blue-filled bars denote the postgraduate students, and the symbol * denotes $p < 0.05$.

Meanwhile, based on these flexible and robust variability metrics per student, the classification of postgraduate students versus junior high school students was further performed by adopting the leave-one-out cross-validation (LOOCV) strategy (Zeng *et al* 2012). Herein, considering m (m = 40 of both postgraduates and junior high school students) samples, in each LOOCV procedure, m-1 subjects were used to training the linear discriminant analysis (LDA) classifier, and the remaining 1 sample was used for testing until all subjects were served as testing for one time. After the LOOCV was finished, the corresponding classification accuracy would be then reported. Here, Fig. 6 displays the scatterplot of flexible and robust variability metrics, which indicated that these metrics could accurately classify both groups, and indeed, the LDA could achieve an accuracy of 92.50% when classifying these subjects by using the variability metrics proposed in this study.

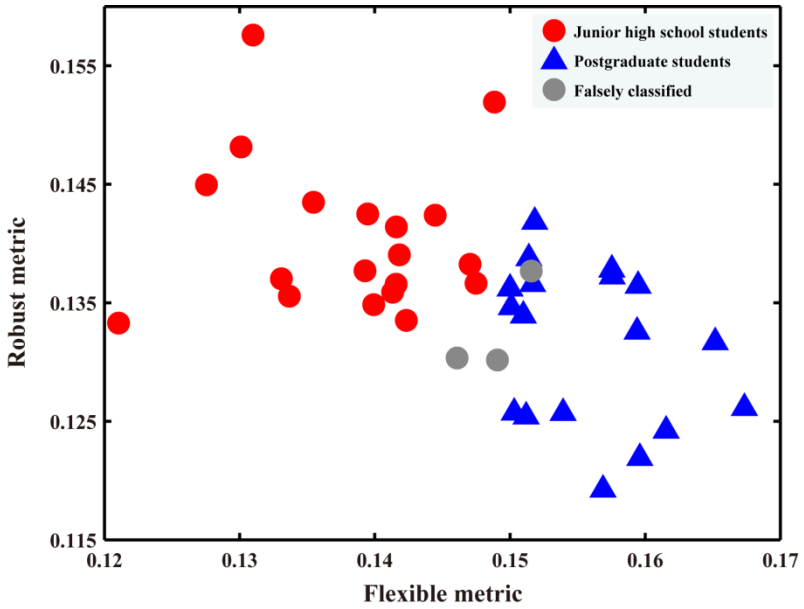

Fig. 6. The scatterplot of flexible and robust network variability metrics. The red-filled circles denote the junior high school students, the blue-filled triangles denote the postgraduates, and the grey-filled circles denote the falsely classified students.

Finally, the potential relationships between individual decision behaviors and network variability for postgraduate students and junior high school students were investigated, and the opposite tendencies of both variables between the two independent groups were displayed in Figs. 7 ~~and 8~~to 10. Concretely, for postgraduate students (Figs. 7 and 8), Fig. 7 showed that the individual decision AR was marginally significantly negative-correlated with the *CC* (r = -0.479, p = 0.060), *GE* (r = -0.489, p = 0.055), *LE* (r = -0.472, p = 0.065), *CPL* (r = -0.435, p = 0.092; CW:), and small-worldness (r = -0.529, p = 0.035). Concerning the CW displayed in Fig. 8, similar tendency was found, as the CW also illustrated the significantly negative relationship with the *CC* (r = -0.488, p = 0.055), *GE* (r = -0.542, p = 0.030), *LE* (r = -0.522, p = 0.038), *CPL* (r = -0.522, p = 0.038), and small-worldness (r = -0.610, p = 0.012).~~In detail, for postgraduate students (Fig. 7), both decision behaviors (i.e., AR and CW) were marginally significantly negative-correlated with the *CC* (AR: r = -0.479, p = 0.060; CW: r = -0.488, p = 0.055), *GE* (AR: r = -0.489, p = 0.055; CW: r = -0.542, p = 0.030), *LE* (AR: r = -0.472, p = 0.065; CW: r = -0.522, p = 0.038), *CPL* (AR: r = -0.435, p = 0.092; CW: r = -0.522, p = 0.038), and small-worldness (AR: r = -0.529, p = 0.035; CW: r = -0.610, p = 0.012).~~

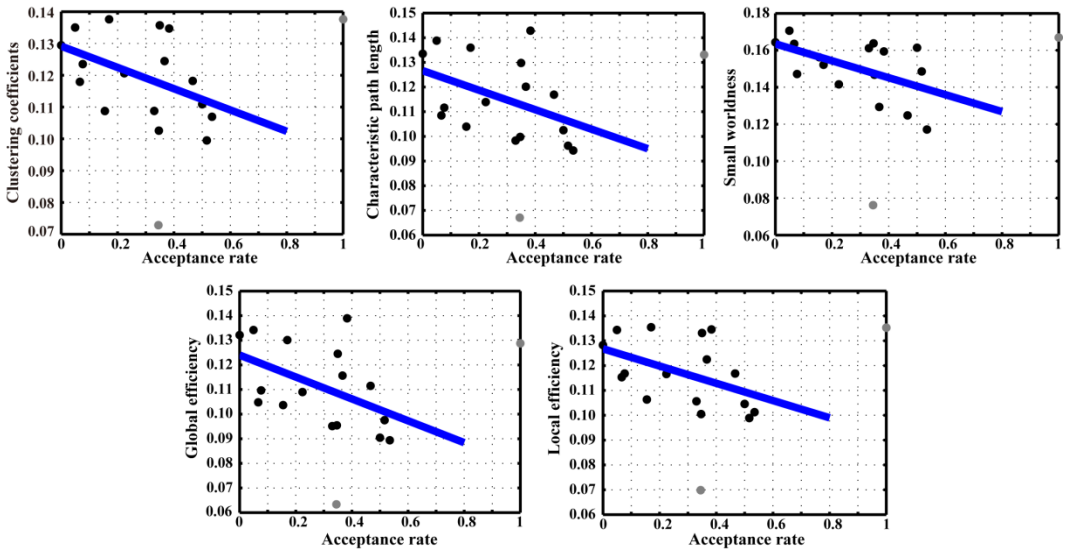

Fig. 7. The relationship between resting-state network variability metrics and the acceptance rate for postgraduate students. In each subfigure, the blue lines denote the fitted linear trend between two variables, the black and grey filled circles denote the included and outlier subjects, respectively.

~~**Fig. 7.** The relationship between resting state network variability and task behavior for postgraduate students. The scatter plots in the first and second row denote the correlations of resting state network variability versus AR and CW, respectively. In each subfigure, the blue lines denote the fitted linear trend between two variables, the black and grey filled circles denote the included and outlier subjects, respectively.~~

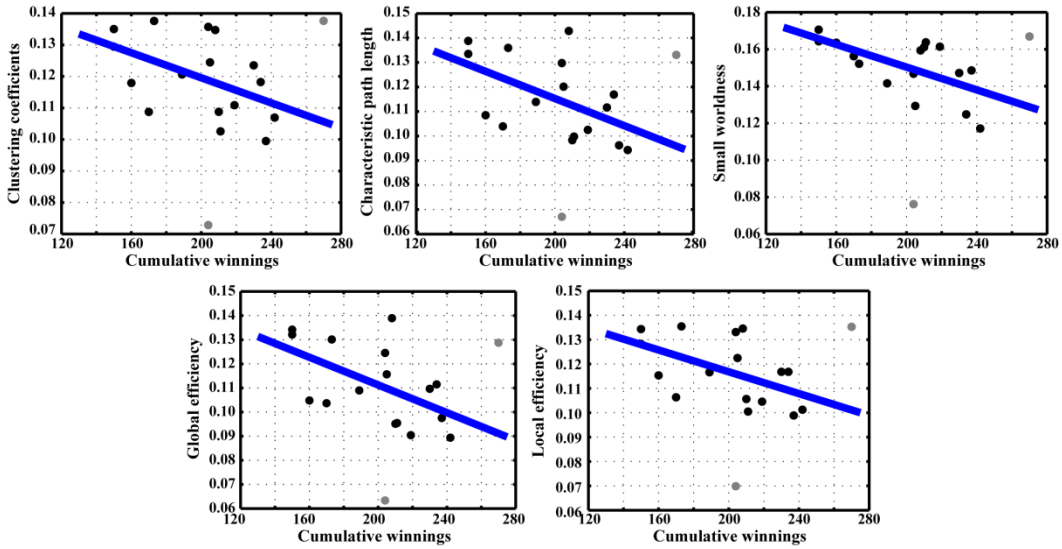

Fig. 8. The relationships between resting-state network variability metrics and the cumulative winnings for postgraduate students. In each subfigure, the blue lines denote the fitted linear trend between two variables; the black- and grey-filled circles denote the included and outlier subjects, respectively.

By contrast, the corresponding relationships between resting-state network variability metrics and individual decision behaviors for the junior high school students were further

displayed in Figs. 9 and 10. In detail, as illustrated in Fig. 9, the *CC* (r = 0.545, p = 0.013), *GE* (r = 0.419, p = 0.066), *LE* (r = 0.516, p = 0.020), *CPL* (r = 0.506, p = 0.023), and small-worldness (r = 0.512, p = 0.021) were found to be significantly and positively related to the decision AR in junior high school students. Concerning the CW in junior high school students, Fig. 10 eventually illustrated that the individual CW also showed the significantly positive relationships with the *CC* (r = 0.634, p = 0.003), *GE* (r = 0.500, p = 0.025), *LE* (r = 0.603, p = 0.005), *CPL* (r = 0.587, p = 0.007), and small-worldness (r = 0.512, p = 0.021) of their resting-state network variability.~~as illustrated in Fig. 8, the *CC* (AR: r = 0.545, p = 0.013; CW: r = 0.634, p = 0.003), *GE* (AR: r = 0.419, p = 0.066; CW: r = 0.500, p = 0.025), *LE* (AR: r = 0.516, p = 0.020; CW: r = 0.603, p = 0.005), *CPL* (AR: r = 0.506, p = 0.023; CW: r = 0.587, p = 0.007), and small-worldness (AR: r = 0.512, p = 0.021; CW: r = 0.512, p = 0.021) were significantly and positively related to the AR and CW in junior high school students.~~

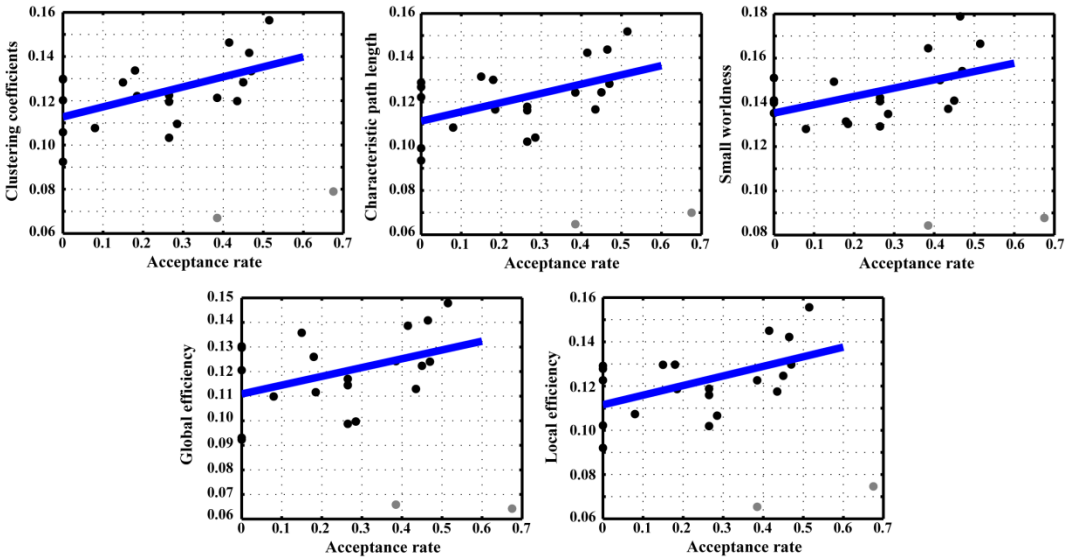

Fig. 9. The relationship between resting-state network variability metrics and the acceptance rate for junior high school students. In each subfigure, the blue lines denote the fitted linear trend between two variables, the black and grey filled circles denote the included and outlier subjects, respectively.

~~**Fig. 8.** The relationship between resting-state network variability and task behavior for junior high school students. The scatter plots in the first and second row denote the correlations of resting-state network variability versus AR and CW, respectively. In each subfigure, the blue lines denote the fitted linear trend between two variables, the black and grey filled circles denote the included and outlier subjects, respectively.~~

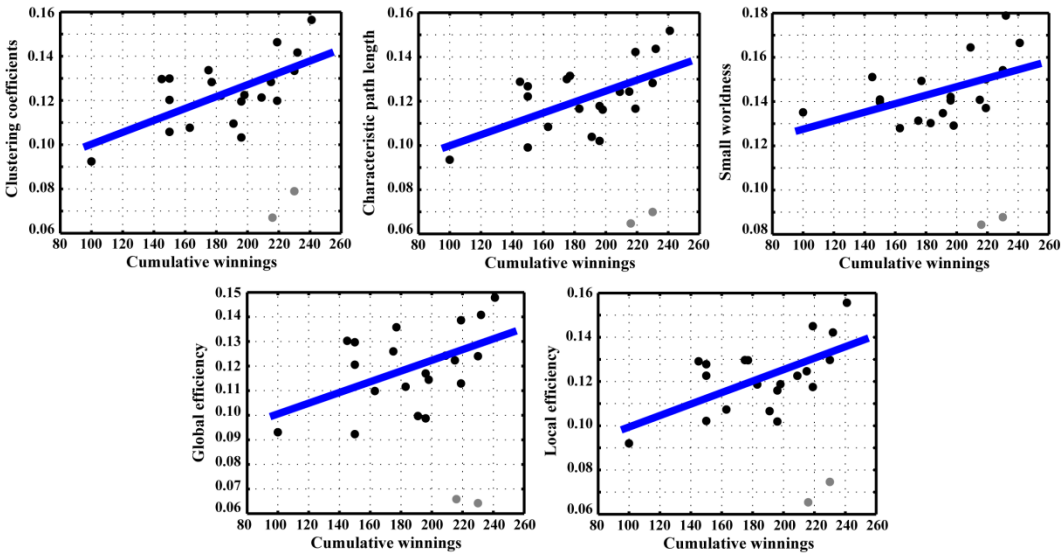

Fig. 10. The relationships between resting-state network variability metrics and the cumulative winnings for junior high school students. In each subfigure, the blue lines denote the fitted linear trend between two variables; the black and grey filled circles denote the included and outlier subjects, respectively.

4. Discussion

When referring to the time-resolved function connectivity, the network connectivity fluctuates in a transient time interval (Hutchison *et al* 2013), and these fluctuations are further found to be related to the modularity of brain network architecture (Pedersen *et al* 2018, Lurie *et al* 2018). Fluctuating temporal variability in network topology corresponds to the varied flexibility in the network architecture, and the flexibility of those edges is believed to effectively index the brain activity (Lurie *et al* 2018, Allen *et al* 2014). Meanwhile, the corresponding temporal flexibility might be measured by the temporal complexity of time-varying functional connectivity in the brain (Pedersen *et al* 2018). The entropy is useful in addressing the randomness (irregularity) of a given system, and higher entropy always associates with higher randomness, as well as the larger complexity. In this study, we thereby used the fuzzy entropy (Chen *et al* 2007, Chen *et al* 2009) to evaluate the fluctuating temporal variability in time-varying resting-state networks and further investigated the possible relationship between the resting-state network variability and individual decision behaviors. In addition, to validate the applicability of fuzzy entropy in capturing the fluctuating temporal variability, we also recorded and further analyzed another independent resting-state EEG dataset before a P300 task by the independent amplifier (i.e., Symtop Instrument, Beijing, China), which also demonstrated the similar flexible and robust resting-state architecture (see APPENDIX).

Just as depicted above, during the simulation study, edge D-E was defined by $MIX(p = 0.5)$ and had the largest complexity; while edge A-C was defined by $MIX(p = 0.1)$ and had the smallest complexity. Fig. 3 demonstrates that in contrast to the other approaches, such as the variance and non-linear test statistic based on the median, only the fuzzy entropy could accurately estimate the network edge complexity in a predefined 5-nodes network. In this study, the fuzzy entropy presented the precise complexity order of the five edges as edge D-E >

edge C-E > edge C-D > edge B-D > edge A-C; nevertheless, the remaining approaches incorrectly identified the opposite tendency among the five edges. In fact, unlike fuzzy entropy, both methods are more concerned about capturing the fluctuation of signal magnitude (Dionisio *et al* 2007), while the fluctuating network pattern is more meaningful to uncover the neural basis of physiological signals. Under some specific situations, they will fail in describing the temporal complexity and even present the opposite tendency. On the contrary, fuzzy entropy is insensitive to the data magnitude (Fig. 3e) but depends more on the data distribution (Dionisio *et al* 2007), thus fuzzy entropy is more helpful to capture the dynamic fluctuations of network patterns. Therefore, we believed the simulation displayed in Fig. 3 effectively validated the applicability of fuzzy entropy in measuring the fluctuating temporal variability of the resting-state networks across time scales.

In essence, when the brain is at rest, along with participants' closing their eyes, the brain functions in an interoceptive state consisting of the imagination and sensory activity (Marx *et al* 2003, Marx *et al* 2004), at the same time, the intrinsic connectivity synchronization that relates to somatosensory (Fox *et al* 1987) and auditory network increases. For both groups, a highly flexible network architecture consistently experienced denser connectivity in the bilateral temporal lobe (Fig. 4a), which reflected that these regions overlapped with that activated by the interoceptive state under the eye-closed resting state. In essence, previous studies have demonstrated that the DMN is the core and inherent network in the brain (Shen 2015), and the dynamics of DMN may serve as the basis when switching between exteroceptive and interoceptive state (Wang *et al* 2015b). DMN relates to the individual internal process, self-generated thought, and mind wandering (Buckner and Vincent 2007, Anticevic *et al* 2012). In this study, for both groups, we consistently showed the DMN-like topology that indexes the robust network architecture, which was measured by fuzzy entropy (Fig. 4b). In essence, the flexibility in functional network connectivity closely relates to its complexity, an increase in edge flexibility corresponds to the higher signal complexity. An interesting issue was that, although the network in a resting state indeed fluctuates in a transient time interval, we could still observe a steady DMN pattern connecting the frontal and occipital lobe. We assumed that this might be the reason why our previous study found a close relationship between the frontal-occipital long-range linkage and P300 (Li *et al* 2015), as well as other findings in related resting-state studies (Jann *et al* 2009, Prestel *et al* 2018).

Decision-making requires an effective evaluation of the current situation, which relies on effectively assessing external (i.e., monetary value) and internal factors (i.e., fairness) (Huerta and Kaas 1990). The decision-making in adults and adolescents is usually influenced by many factors including inhibitory control, learning, emotion, and social context (Gladwin *et al* 2011, Rubia *et al* 2000), and distinctive decision behaviors between the two groups have been found in our previous study (Si *et al* 2020b). While time-resolved investigation allows the fine-grained evaluations of the relationship between functional connectivity and ongoing cognition (Pedersen *et al* 2018), such as decision-making. In our present study, based on the identified flexible and robust architectures displayed in Fig. 4, the statistics of flexible and robust variability metrics were first completed (Fig. 5), which showed significant differences between the postgraduate students and junior high school students ($p < 0.05$). And when using the flexible and robust variability metrics to classify the two groups, an accuracy of 92.50% could be achieved (Fig. 6), while if only the raw coherence metrics were used, no satisfying

results would be obtained, which further validated the capacity of the proposed protocols in capturing the fluctuating temporal variability in resting-state networks, as well as identifying distinct groups.

~~In fact, the studies focusing on childhood development and socialization have confirmed the increase of the preference for fair distribution along with their growing up (Marchetti *et al* 2019, Castelli *et al* 2014). That is, compared to the adults, the adolescents were more likely to accept the offer given by the others since they (i.e., children and adolescents) preferred the outcome, which led to a large AR even when faced with unfair offers; nevertheless, the adults focused on the intention, which might explain the high rejection rates related to unfair offers in the postgraduate students. In our present study, the potential relationships between decision behavior and network variability of both groups were thus investigated, to uncover if the different decision strategies were used by both groups in the UG task.~~

Quantitatively, small-worldness reflects regional specialization and information transfer efficiency of a given network, the *CC* and *LE* are the aggregation of the node and reflect the capacity for specialized processing of the local region; by contrast, the *CPL* and *GE* denote the functional integration of multiple brain regions, and all of these parameters can effectively evaluate the efficiency related to the specific information processing in the brain (Cozzo *et al* 2015). In this study, the temporal fuzzy entropy of these parameters (i.e., *CC*, *GE*, *LE*, *CPL*, and small-worldness) is thought to has the potential to quantitatively measure the local and global flexibility in the brain. As displayed in Figs. 7 to 10, what is interesting was the opposite decision-making behaviors between adolescents and adults under unfair conditions. In particular, in postgraduate students, we found the network variability parameters were negatively related to both AR and CW (Figs. 7 and 8), while the opposite relationships were found in junior high school students as these parameters were significantly positively related to individual AR and CW (Figs. ~~8~~9 and 10). A small AR means an individual prefers fairness by rejecting the current unfair offer to punish the unfair behavior of the proposer (Yamagishi *et al* 2009), which thus leads to the lower task earning (i.e., smaller CW). In fact, the studies focusing on childhood development and socialization have primarily confirmed the increase of the preference for fairness from adolescence to adulthood (Marchetti *et al* 2019, Castelli *et al* 2014). Along with their growing up, the individuals' sociality increases and they are increasingly capable of using a multi-dimensional rule to deal with the current decision situation (van Duijvenvoorde *et al* 2010). Since this study was the first work to explore the potential relationships between resting-state brain network variability and individual decision behaviors, based on these considerations mentioned above, we believed that compared to those postgraduate students, junior high school students were more likely to accept the offer given by the others, even those unfair ones, as they preferred current interests over fairness (Si *et al* 2020b). By contrast, the postgraduate students focused more on the intention and preferred the fairness (Peterburs *et al* 2017), if the unfairness occurs, they would like to reject the unfair offer in this situation. This might lead to a large AR in junior high school students but the high rejection rates in postgraduate students, as well as the opposite relationships between network variability and decision behaviors for both groups.

~~That is, compared to the adults, the adolescents were more likely to accept the offer given by the others since they (i.e., children and adolescents) preferred the outcome, which led to a large AR even when faced with unfair offers; nevertheless, the adults focused on the~~

~~intention, which might explain the high rejection rates related to unfair offers in the postgraduate students. In our present study, the potential relationships between decision behavior and network variability of both groups were thus investigated, to uncover if the different decision strategies were used by both groups in the UG task.~~

~~Based on the considerations above, we believed that compared to the postgraduate students, the junior high school students pay more attention to monetary value but less to fairness; even when meeting with unfair conditions, the adolescents tend to accept the unfairness to ensure their self interest. Nevertheless, the postgraduate students incline to assess the fairness of the current situation, if the unfairness occurs, they would like to reject the unfair offer in this situation, which then results in an opposite relationship between network variability and task behavior with the junior high school students.~~

One possible limitation of this study would be that although sparse electrodes could reduce the effect of volume conduction on EEG and related networks, theoretically, EEG source localization could eliminate the volume conduction effect by projecting scalp EEG back to the cortex. In the future, by performing the EEG source localization, we will further investigate the fluctuating temporal variability of brain networks on the cortical layer, to further uncover the neural basis of network variability and its relationships with human cognition.

~~One possible limitation of this study would be that although sparse electrodes could reduce the effect of volume conduction on EEG and related networks, theoretically, EEG inverse solution could eliminate the volume conduction effect by projecting scalp EEG back to the cortex. And in the future, by adopting the EEG inverse solution, we will further investigate the fluctuating temporal variability of brain networks on the cortical layer, to further uncover the neural basis of network variability and its relationships with human cognition.~~

5. Conclusion

In summary, our present study first validated the capacity of fuzzy entropy in quantitatively measuring the fluctuating temporal patterns of the time-varying resting-state brain networks. When applying in the decision-making and P300 EEG datasets, the corresponding inherent fluctuating temporal patterns of resting-state networks were effectively captured; in particular, the flexible and robust architectures of the brain at rest were identified and distributed at the bilateral temporal lobe and frontal/occipital lobe, respectively. Moreover, the corresponding variability metrics not only helped differentiate different groups but also closely related to the individual decision behaviors, which could facilitate our knowledge of the human cognitive process, such as decision-making.

Acknowledgments

Appendix

Conventional approaches

In essence, the variance (also the standard-deviation) , as a straightforward method, has been used to measure the uncertainty of a given signal (Dionisio *et al* 2007), which is usually in the resting-state fMRI studies (Hindriks *et al* 2016, Sakoglu *et al* 2010). In addition, Zalesky and colleagues also used the univariate test statistic to measure the time-varying correlation coefficient fluctuations for pairwise regions (Zalesky *et al* 2014). In this study, to first validate the benefits of the fuzzy entropy, these two traditional methods i.e., the variance and non-linear test statistic, were also used to estimate the corresponding temporal complexity of the simulated network edges, and the corresponding performance of the fuzzy entropy was then statistically compared with that of the two traditional methods. Here, the corresponding definitions of both methods were further depicted below.

Concerning ~~In the current study, we, therefore, also proposed to use the traditional test statistics, i.e., the variance and non-linear test statistic, to estimate the temporal complexity of the defined network edges. On the one hand,~~ the variance, V, for each of the five network edges is formulized as follow;

$$V = \frac{1}{L-1}\sum_{i=1}^{L}(p_i - \mu)^2 \tag{A1}$$

where $p = p_1, p_2, \ldots, p_L$ denotes the time series of the simulated network edge, V denotes the variance of the time series, and μ denotes the mean of the signal.

For the non-linear test statistic, let m be the median of p and let $n_1, n_2, \ldots, n_J$ be the samples for which p crosses m. p then makes J-1 consecutive excursions from m. The length I_n and height H_n of the j-th excursion are defined as $I_n = n_{j+1} - n_j$ and $H_n = max\{|p_i - m| : n_j < i < n_{j+1}\}$, respectively. The non-linear test statistic (Zalesky *et al* 2014, Hindriks *et al* 2016) is finally defined as,

$$\xi = \sum_{j=1}^{J-1} \left| I_j^{\alpha} H_j^{\beta} \right| \tag{A2}$$

where α and β control the relative weighting of the length and height for each excursion. Meanwhile, following Zalesky and colleagues (Zalesky *et al* 2014), in this study, we then set $\alpha = 0.9$ and $\beta = 1$.

Validation on resting-state P300 EEG

Aiming to validate its applicability, the independent group of resting-state EEG datasets recorded before an oddball P300 task (Li *et al* 2019) was further analyzed by applying the same analytical protocols.

After being preprocessed with the same analytical protocols, 19 healthy right-handed participants (6 females, age range of 20-41 years, and mean 29.37 years) were included in the following analysis. They had the normal or corrected-to-normal visual acuity, and none of them had histories of substance abuse, took the medication with deleterious effects on cognition, and had a neurological illness.

Their resting-state EEG datasets were recorded using the Symtop amplifier (Symtop Instrument, Beijing, China) and a 16-channel Ag/AgCl electrode cap (BrainMaster, Inc., Shenzhen, China), whose electrodes (Fp1/2, F3/4, C3/C4, P3/4, O1/2, F7/8, T3/4/5/6) were positioned according to the 10-20 international electrode system. Electrode AFz served as the reference. The predefined sampling rate is 1,000 Hz and the online bandpass filtering is

0.05-100 Hz. The impedance per electrode was kept below 5 KΩ throughout the experiment.

Fig. A1 displays the network edges with the 20% largest (i.e., flexible, Fig. A1a) and 20% smallest (i.e., robust, Fig. A1b) fuzzy entropy, respectively, as well as the corresponding nodal degree ~~ND~~ distribution (Fig. A1c). Coincided with the findings of the postgraduate students and junior high school students in the UG task, the flexible architectures were also distributed at the bilateral temporal lobe (Fig. A1a), whose electrodes were printed with deep red color in Fig. A1c. Meanwhile, Fig. A1b further illustrates a robust DMN-like architecture, which linked the frontal and occipital lobe (i.e., the electrodes with deep blue color in Fig. A1c).

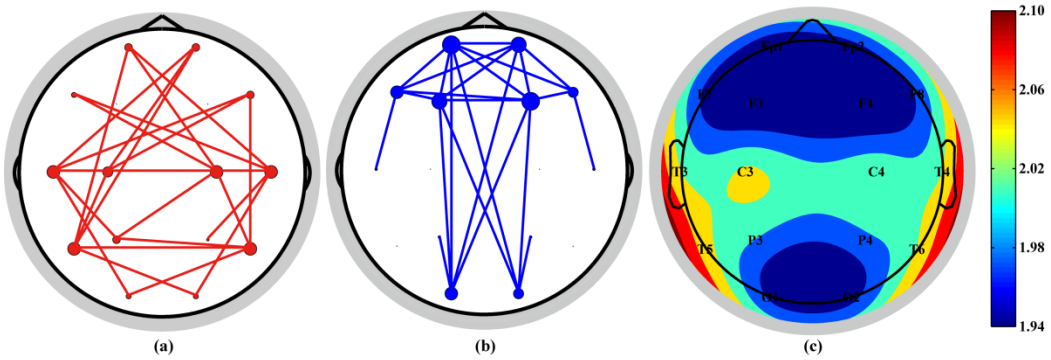

Fig. A1. Scalp topologies with the 20% largest and smallest fuzzy entropy for resting P300. (a) Flexible architecture, (b) Robust architecture, and (c) Nodal degree ~~ND~~ distribution. In subfigures (a, b), the size of each electrode is proportional to its binary degree in the 20% largest and smallest network, respectively.

References

Abasolo D, Hornero, R, Espino, P, Alvarez, D,Poza, J 2006 Entropy analysis of the EEG background activity in Alzheimer's disease patients *Physiol Meas* **27** 241-53.

Acharya U R, Fujita, H, Sudarshan, V K, Bhat, S,Koh, J E W 2015 Application of entropies for automated diagnosis of epilepsy using EEG signals: A review *Knowl-Based Syst* **88** 85-96.

Allen E A, Damaraju, E, Plis, S M, Erhardt, E B, Eichele, T,Calhoun, V D 2014 Tracking whole-brain connectivity dynamics in the resting state *Cereb Cortex* **24** 663-76.

Anticevic A, Cole, M W, Murray, J D, Corlett, P R, Wang, X J,Krystal, J H 2012 The role of default network deactivation in cognition and disease *Trends Cogn Sci* **16** 584-92.

Bassett D S,Bullmore, E T 2017 Small-World Brain Networks Revisited *Neuroscientist* **23** 499-516.

Betzel R F, Fukushima, M, He, Y, Zuo, X N,Sporns, O 2016 Dynamic fluctuations coincide with periods of high and low modularity in resting-state functional brain networks *NeuroImage* **127** 287-97.

Bledowski C, Prvulovic, D, Hoechstetter, K, Scherg, M, Wibral, M, Goebel, R,Linden, D E 2004 Localizing P300 generators in visual target and distractor processing: a combined event-related potential and functional magnetic resonance imaging study *J Neurosci* **24** 9353-60.

Braun U, Schafer, A, Walter, H, Erk, S, Romanczuk-Seiferth, N, Haddad, L, Schweiger, J I, Grimm, O, Heinz, A, Tost, H, Meyer-Lindenberg, A,Bassett, D S 2015 Dynamic

reconfiguration of frontal brain networks during executive cognition in humans *Proc Natl Acad Sci USA* **112** 11678-83.

Buckner R L,Vincent, J L 2007 Unrest at rest: Default activity and spontaneous network correlations *NeuroImage* **37** 1091-6.

Cao Z, Lai, K L, Lin, C T, Chuang, C H, Chou, C C,Wang, S J 2018 Exploring resting-state EEG complexity before migraine attacks *Cephalalgia* **38** 1296-306.

Cao Z, Lin, C-T, Lai, K-L, Ko, L-W, King, J-T, Liao, K-K, Fuh, J-L,Wang, S-J 2020 Extraction of SSVEPs-Based Inherent Fuzzy Entropy Using a Wearable Headband EEG in Migraine Patients *IEEE Transactions on Fuzzy Systems* **28** 14-27.

Cao Z H,Lin, C T 2018 Inherent Fuzzy Entropy for the Improvement of EEG Complexity Evaluation *IEEE Trans Fuzzy Syst* **26** 1032-5.

Castelli I, Massaro, D, Sanfey, A G,Marchetti, A 2010 Fairness and intentionality in children's decision-making *Int Rev Econ* **57** 269-88.

Castelli I, Massaro, D, Sanfey, A G,Marchetti, A 2014 "What is fair for you?" Judgments and decisions about fairness and Theory of Mind *Eur J Dev Psychol* **11** 49-62.

Cecchetto C, Korb, S, Rumiati, R I,Aiello, M 2017 Emotional reactions in moral decision-making are influenced by empathy and alexithymia *Soc Neurosci-UK* 1-15.

Chen W, Wang, Z, Xie, H,Yu, W 2007 Characterization of surface EMG signal based on fuzzy entropy *IEEE Trans Neural Syst Rehabil Eng* **15** 266-72.

Chen W, Zhuang, J, Yu, W,Wang, Z 2009 Measuring complexity using FuzzyEn, ApEn, and SampEn *Med Eng Phys* **31** 61-8.

Cozzo E, Kivela, M, De Domenico, M, Sole-Ribalta, A, Arenas, A, Gomez, S, Porter, M A,Moreno, Y 2015 Structure of triadic relations in multiplex networks *New J Phys* **17**.

Damoiseaux J, Rombouts, S, Barkhof, F, Scheltens, P, Stam, C, Smith, S M,Beckmann, C 2006 Consistent resting-state networks across healthy subjects *Proc Natl Acad Sci USA* **103** 13848-53.

Dimitrakopoulos G N, Kakkos, I, Dai, Z, Wang, H, Sgarbas, K, Thakor, N, Bezerianos, A,Sun, Y 2018 Functional Connectivity Analysis of Mental Fatigue Reveals Different Network Topological Alterations Between Driving and Vigilance Tasks *IEEE Trans Neural Syst Rehabil Eng* **26** 740-9.

Dionisio A, Menezes, R,Mendes, D A 2007 Entropy and uncertainty analysis in financial markets *arXiv preprint*.

Dong L, Li, F, Liu, Q, Wen, X, Lai, Y, Xu, P,Yao, D 2017 MATLAB Toolboxes for Reference Electrode Standardization Technique (REST) of Scalp EEG *Front Neurosci* **11** 601.

Falahpour M, Chang, C, Wong, C W,Liu, T T 2018 Template-based prediction of vigilance fluctuations in resting-state fMRI *NeuroImage* **174** 317-27.

Fox P T, Burton, H,Raichle, M E 1987 Mapping human somatosensory cortex with positron emission tomography *J Neurosurg* **67** 34-43.

Gao J B, Hu, J, Liu, F Y,Cao, Y H 2015 Multiscale entropy analysis of biological signals: a fundamental bi-scaling law *Front Comput Neurosci* **9**.

Garrett D D, Kovacevic, N, Mcintosh, A R,Grady, C L 2011 The Importance of Being Variable *J Neurosci* **31** 4496-503.

Gladwin T E, Figner, B, Crone, E A,Wiers, R W 2011 Addiction, adolescence, and the integration of control and motivation *Dev Cogn Neurosci* **1** 364-76.

Guroglu B, Van Den Bos, W,Crone, E A 2009 Fairness considerations: increasing understanding of intentionality during adolescence *J Exp Child Psychol* **104** 398-409.

He T, Clifford, G,Tarassenko, L 2005 Application of independent component analysis in removing artefacts from the electrocardiogram *Neural Computing and Applications* **15** 105-16.

Hearne L J, Cocchi, L, Zalesky, A,Mattingley, J B 2017 Reconfiguration of Brain Network Architectures between Resting-State and Complexity-Dependent Cognitive Reasoning *Journal of Neuroscience* **37** 8399-411.

Hindriks R, Adhikari, M H, Murayama, Y, Ganzetti, M, Mantini, D, Logothetis, N K,Deco, G 2016 Can sliding-window correlations reveal dynamic functional connectivity in resting-state fMRI? *NeuroImage* **127** 242-56.

Hoffmann R,Tee, J-Y 2006 Adolescent–adult interactions and culture in the ultimatum game *J Econ Psychol* **27** 98-116.

Huang Y, Zhang, J, Cui, Y, Yang, G, He, L, Liu, Q,Yin, G 2017 How Different EEG References Influence Sensor Level Functional Connectivity Graphs *Front Neurosci* **11** 368.

Huerta M F,Kaas, J H 1990 Supplementary Eye Field as Defined by Intracortical Microstimulation - Connections in Macaques *J Comp Neurol* **293** 299-330.

Hutchison R M, Womelsdorf, T, Allen, E A, Bandettini, P A, Calhoun, V D, Corbetta, M, Della Penna, S, Duyn, J H, Glover, G H, Gonzalez-Castillo, J, Handwerker, D A, Keilholz, S, Kiviniemi, V, Leopold, D A, De Pasquale, F, Sporns, O, Walter, M,Chang, C 2013 Dynamic functional connectivity: promise, issues, and interpretations *NeuroImage* **80** 360-78.

Jann K, Dierks, T, Boesch, C, Kottlow, M, Strik, W,Koenig, T 2009 BOLD correlates of EEG alpha phase-locking and the fMRI default mode network *NeuroImage* **45** 903-16.

Jiang Y, Tian, Y,Wang, Z 2019 Causal Interactions in Human Amygdala Cortical Networks across the Lifespan *Sci Rep* **9** 5927.

Kim B M, Lee, J, Choi, A R, Chung, S J, Park, M, Koo, J W, Kang, U G,Choi, J S 2021 Event-related brain response to visual cues in individuals with Internet gaming disorder: relevance to attentional bias and decision-making *Transl Psychiatry* **11** 258.

Li F, Liu, T, Wang, F, Li, H, Gong, D, Zhang, R, Jiang, Y, Tian, Y, Guo, D,Yao, D 2015 Relationships between the resting-state network and the P3: Evidence from a scalp EEG study *Sci Rep* **5** 15129.

Li F, Tao, Q, Peng, W, Zhang, T, Si, Y, Zhang, Y, Yi, C, Biswal, B, Yao, D,Xu, P 2020 Inter-subject P300 variability relates to the efficiency of brain networks reconfigured from resting-to task-state: Evidence from a simultaneous event-related EEG-fMRI study *NeuroImage* **205** 116285.

Li F, Wang, J, Liao, Y, Yi, C, Jiang, Y, Si, Y, Peng, W, Yao, D, Zhang, Y, Dong, W,Xu, P 2019 Differentiation of Schizophrenia by Combining the Spatial EEG Brain Network Patterns of Rest and Task P300 *IEEE Trans Neural Syst Rehabil Eng* **27** 594-602.

Li N, Ma, N, Liu, Y, He, X S, Sun, D L, Fu, X M, Zhang, X C, Han, S H,Zhang, D R 2013a Resting-State Functional Connectivity Predicts Impulsivity in Economic Decision-Making *J Neurosci* **33** 4886-95.

Li P, Liu, C, Wang, X, Li, B, Che, W,Liu, C 2013b. Cross-Sample Entropy and Cross-Fuzzy

Entropy for Testing Pattern Synchrony: How Results Vary with Different Threshold Value r. *World Congress on Medical Physics and Biomedical Engineering May 26-31, 2012, Beijing, China.*

Li Y, Pan, J, Wang, F,Yu, Z 2013c A hybrid BCI system combining P300 and SSVEP and its application to wheelchair control *IEEE Trans Biomed Eng* **60** 3156-66.

Long J, Li, Y, Wang, H, Yu, T, Pan, J,Li, F 2012 A hybrid brain computer interface to control the direction and speed of a simulated or real wheelchair *IEEE Trans Neural Syst Rehab Eng* **20** 720-9.

Lurie D, Kessler, D, Bassett, D, Betzel, R F, Breakspear, M, Keilholz, S, Kucyi, A, Liégeois, R, Lindquist, M A,Mcintosh, A R 2018 On the nature of resting fMRI and time-varying functional connectivity.

Mantini D, Perrucci, M G, Del Gratta, C, Romani, G L,Corbetta, M 2007 Electrophysiological signatures of resting state networks in the human brain *Proc Natl Acad Sci USA* **104** 13170-5.

Marchetti A, Baglio, F, Castelli, I, Griffanti, L, Nemni, R, Rossetto, F, Valle, A, Zanette, M,Massaro, D 2019 Social Decision Making in Adolescents and Young Adults: Evidence From the Ultimatum Game and Cognitive Biases *Psychol Rep* **122** 135-54.

Marx E, Deutschlander, A, Stephan, T, Dieterich, M, Wiesmann, M,Brandt, T 2004 Eyes open and eyes closed as rest conditions: impact on brain activation patterns *NeuroImage* **21** 1818-24.

Marx E, Stephan, T, Nolte, A, Deutschlander, A, Seelos, K C, Dieterich, M,Brandt, T 2003 Eye closure in darkness animates sensory systems *NeuroImage* **19** 924-34.

Masulli P, Masulli, F, Rovetta, S, Lintas, A,Villa, A E P 2020 Fuzzy Clustering for Exploratory Analysis of EEG Event-Related Potentials *IEEE Transactions on Fuzzy Systems* **28** 28-38.

Moon S E, Chen, C J, Hsieh, C J, Wang, J L,Lee, J S 2020 Emotional EEG classification using connectivity features and convolutional neural networks *Neural Networks* **132** 96-107.

Northoff G, Qin, P M,Nakao, T 2010 Rest-stimulus interaction in the brain: a review *Trends Neurosci* **33** 277-84.

Pedersen M, Zalesky, A, Omidvarnia, A,Jackson, G D 2018 Multilayer network switching rate predicts brain performance *Proc Natl Acad Sci USA* **115** 13376-81.

Pena-Gomez C, Avena-Koenigsberger, A, Sepulcre, J,Sporns, O 2018 Spatiotemporal Network Markers of Individual Variability in the Human Functional Connectome *Cereb Cortex* **28** 2922-34.

Peterburs J, Voegler, R, Liepelt, R, Schulze, A, Wilhelm, S, Ocklenburg, S,Straube, T 2017 Processing of fair and unfair offers in the ultimatum game under social observation *Sci Rep* **7** 44062.

Pincus S 1995 Approximate Entropy (Apen) as a Complexity Measure *Chaos* **5** 110-7.

Pincus S M 1991 Approximate Entropy as a Measure of System-Complexity *Proc Natl Acad Sci USA* **88** 2297-301.

Pincus S M,Goldberger, A L 1994 Physiological time-series analysis: what does regularity quantify? *Am J Physiol* **266** H1643-56.

Polich J 2007 Updating P300: an integrative theory of P3a and P3b *Clin Neurophysiol* **118**

2128-48.

Prestel M, Steinfath, T P, Tremmel, M, Stark, R,Ott, U 2018 fMRI BOLD Correlates of EEG Independent Components: Spatial Correspondence With the Default Mode Network *Front Hum Neurosci* **12**.

Preuss N, Brändle, L S, Hager, O M, Haynes, M, Fischbacher, U,Hasler, G 2016 Inconsistency and social decision making in patients with Borderline Personality Disorder *Psychiat Res* **243** 115-22.

Qin Y, Xu, P,Yao, D 2010 A comparative study of different references for EEG default mode network: the use of the infinity reference *Clin Neurophysiol* **121** 1981-91.

Rubia K, Overmeyer, S, Taylor, E, Brammer, M, Williams, S C R, Simmons, A, Andrew, C,Bullmore, E T 2000 Functional frontalisation with age: mapping neurodevelopmental trajectories with fMRI *Neurosci Biobehav Rev* **24** 13-9.

Rubinov M,Sporns, O 2010 Complex network measures of brain connectivity: uses and interpretations *NeuroImage* **52** 1059-69.

Sakoglu U, Pearlson, G D, Kiehl, K A, Wang, Y M, Michael, A M,Calhoun, V D 2010 A method for evaluating dynamic functional network connectivity and task-modulation: application to schizophrenia *Magn Reson Mater Phy* **23** 351-66.

Shen H H 2015 Core Concept: Resting-state connectivity *Proc Natl Acad Sci USA* **112** 14115-6.

Shirer W R, Ryali, S, Rykhlevskaia, E, Menon, V,Greicius, M D 2012 Decoding subject-driven cognitive states with whole-brain connectivity patterns *Cereb Cortex* **22** 158-65.

Si Y, Jiang, L, Tao, Q, Chen, C, Li, F, Jiang, Y, Zhang, T, Cao, X, Wan, F, Yao, D,Xu, P 2019a Predicting individual decision-making responses based on the functional connectivity of resting-state EEG *J Neural Eng* **16** 066025.

Si Y, Li, F, Duan, K, Tao, Q, Li, C, Cao, Z, Zhang, Y, Biswal, B, Li, P, Yao, D,Xu, P 2020a Predicting individual decision-making responses based on single-trial EEG *NeuroImage* **206** 116333.

Si Y, Li, F, Li, F, Tu, J, Yi, C, Tao, Q, Zhang, X, Pei, C, Gao, S, Yao, D,Xu, P 2020b The Growing from Adolescence to Adulthood Influences the Decision Strategy to Unfair Situations *IEEE Trans Cogn Dev Syst* 1-.

Si Y, Wu, X, Li, F, Zhang, L, Duan, K, Li, P, Song, L, Jiang, Y, Zhang, T, Zhang, Y, Chen, J, Gao, S, Biswal, B, Yao, D,Xu, P 2019b Different Decision-Making Responses Occupy Different Brain Networks for Information Processing: A Study Based on EEG and TMS *Cereb Cortex* **29** 4119-29.

Simons S, Espino, P,Abásolo, D 2018 Fuzzy Entropy Analysis of the Electroencephalogram in Patients with Alzheimer's Disease: Is the Method Superior to Sample Entropy? *Entropy* **20**.

Sun J, Liu, Z, Rolls, E T, Chen, Q, Yao, Y, Yang, W, Wei, D, Zhang, Q, Zhang, J, Feng, J,Qiu, J 2019 Verbal Creativity Correlates with the Temporal Variability of Brain Networks During the Resting State *Cereb Cortex* **29** 1047-58.

Sutter M 2007 Outcomes versus intentions: On the nature of fair behavior and its development with age *J Econ Psychol* **28** 69-78.

Takahashi T, Cho, R Y, Mizuno, T, Kikuchi, M, Murata, T, Takahashi, K,Wada, Y 2010

Antipsychotics reverse abnormal EEG complexity in drug-naive schizophrenia: A multiscale entropy analysis *NeuroImage* **51** 173-82.

Thompson W H, Brantefors, P,Fransson, P 2017 From static to temporal network theory: Applications to functional brain connectivity *Netw Neurosci* **1** 69-99.

Tian Y, Yang, L, Chen, S F, Guo, D Q, Ding, Z C, Tam, K Y,Yao, D Z 2017a Causal interactions in resting-state networks predict perceived loneliness *Plos One* **12**.

Tian Y, Zhang, H, Jiang, Y, Li, P,Li, Y 2019 A Fusion Feature for Enhancing the Performance of Classification in Working Memory Load With Single-Trial Detection *IEEE Trans Neural Syst Rehabil Eng* **27** 1985-93.

Tian Y, Zhang, H, Xu, W, Zhang, H, Yang, L, Zheng, S,Shi, Y 2017b Spectral Entropy Can Predict Changes of Working Memory Performance Reduced by Short-Time Training in the Delayed-Match-to-Sample Task *Front Hum Neurosci* **11** 437.

Turetsky B I, Dress, E M, Braff, D L, Calkins, M E, Green, M F, Greenwood, T A, Gur, R E, Gur, R C, Lazzeroni, L C,Nuechterlein, K H 2015 The utility of P300 as a schizophrenia endophenotype and predictive biomarker: clinical and socio-demographic modulators in COGS-2 *Schizophr Res* **163** 53-62.

Van Duijvenvoorde A C, Jansen, B R, Visser, I,Huizenga, H M 2010 Affective and cognitive decision-making in adolescents *Dev Neuropsychol* **35** 539-54.

Villafaina S, Collado-Mateo, D, Cano-Plasencia, R, Gusi, N,Fuentes, J P 2019 Electroencephalographic response of chess players in decision-making processes under time pressure *Physiol Behav* **198** 140-3.

Wang H, Xu, G, Wang, X, Sun, C, Zhu, B, Fan, M, Jia, J, Guo, X,Sun, L 2019 The reorganization of resting-state brain networks associated with motor imagery training in chronic stroke patients *IEEE Trans Neural Syst Rehabil Eng*.

Wang L, Zheng, J, Huang, S,Sun, H 2015a P300 and Decision Making under Risk and Ambiguity *Comput Intell Neurosci* **2015** 108417.

Wang X H, Li, L H, Xu, T,Ding, Z X 2015b Investigating the Temporal Patterns within and between Intrinsic Connectivity Networks under Eyes-Open and Eyes-Closed Resting States: A Dynamical Functional Connectivity Study Based on Phase Synchronization *Plos One* **10**.

Wang Y, Zhang, Z, Bai, L, Lin, C, Osinsky, R,Hewig, J 2017 Ingroup/outgroup membership modulates fairness consideration: neural signatures from ERPs and EEG oscillations *Sci Rep* **7** 39827.

Xiang J, Li, C G, Li, H F, Cao, R, Wang, B, Han, X H,Chen, J J 2015 The detection of epileptic seizure signals based on fuzzy entropy *J Neurosci Methods* **243** 18-25.

Xie H B, Zheng, Y P, Guo, J Y,Chen, X 2010 Cross-fuzzy entropy: A new method to test pattern synchrony of bivariate time series *Information Sciences* **180** 1715-24.

Yamagishi T, Horita, Y, Takagishi, H, Shinada, M, Tanida, S,Cook, K S 2009 The private rejection of unfair offers and emotional commitment *Proc Natl Acad Sci USA* **106** 11520-3.

Yang A C, Hong, C J, Liou, Y J, Huang, K L, Huang, C C, Liu, M E, Lo, M T, Huang, N E, Peng, C K, Lin, C P,Tsai, S J 2015 Decreased Resting-State Brain Activity Complexity in Schizophrenia Characterized by Both Increased Regularity and Randomness *Hum Brain Mapp* **36** 2174-86.

Yao D 2001 A method to standardize a reference of scalp EEG recordings to a point at infinity *Physiol Meas* **22** 693.

Yu H, Lei, X, Song, Z, Liu, C,Wang, J 2020 Supervised Network-Based Fuzzy Learning of EEG Signals for Alzheimer's Disease Identification *IEEE Trans Fuzzy Syst* **28** 60-71.

Yu H, Wu, X, Cai, L, Deng, B,Wang, J 2018 Modulation of Spectral Power and Functional Connectivity in Human Brain by Acupuncture Stimulation *IEEE Trans Neural Syst Rehabil Eng* **26** 977-86.

Yu Q, Erhardt, E B, Sui, J, Du, Y, He, H, Hjelm, D, Cetin, M S, Rachakonda, S, Miller, R L, Pearlson, G,Calhoun, V D 2015 Assessing dynamic brain graphs of time-varying connectivity in fMRI data: application to healthy controls and patients with schizophrenia *NeuroImage* **107** 345-55.

Zalesky A, Fornito, A, Cocchi, L, Gollo, L L,Breakspear, M 2014 Time-resolved resting-state brain networks *Proc Natl Acad Sci USA* **111** 10341-6.

Zeng L, Shen, H, Liu, L, Wang, L, Li, B, Fang, P, Zhou, Z, Li, Y,Hu, D 2012 Identifying major depression using whole-brain functional connectivity: a multivariate pattern analysis *Brain* **135** 1498-507.

Zhang R, Yao, D, Valdés-Sosa, P A, Li, F, Li, P, Zhang, T, Ma, T, Li, Y,Xu, P 2015 Efficient resting-state EEG network facilitates motor imagery performance *J Neural Eng* **12** 066024.

Zhou G, Liu, P, He, J, Dong, M, Yang, X, Hou, B, Von Deneen, K, Qin, W,Tian, J 2012 Interindividual reaction time variability is related to resting-state network topology: an electroencephalogram study *Neuroscience* **202** 276-82.

Brain variability in dynamic resting-state networks identified by fuzzy entropy: a scalp EEG study

Fali Li[1,2], Lin Jiang[2], Yuanyuan Liao[2], Yajing Si[3,1], Chanli Yi[2], Yangsong Zhang[4], Xianjun Zhu[5,6], Zhenglin Yang[5,6], Dezhong Yao[1,2], Zehong Cao[7], Peng Xu[1,2]*

[1]The Clinical Hospital of Chengdu Brain Science Institute, MOE Key Lab for Neuroinformation, University of Electronic Science and Technology of China, Chengdu, 611731, China

[2]School of Life Science and Technology, Center for Information in Medicine, University of Electronic Science and Technology of China, Chengdu, 611731, China

[3]School School of Psychology, Xinxiang Medical University, Xinxiang, 453003, China

[4]School of Computer Science and Technology, Southwest University of Science and Technology, Mianyang, 621010, China

[5]The Sichuan Provincial Key Laboratory for Human Disease Gene Study, Prenatal Diagnosis Center, Sichuan Provincial People's Hospital, University of Electronic Science and Technology of China, Chengdu, China

[6]Research Unit for Blindness Prevention of Chinese Academy of Medical Sciences (2019RU026), Sichuan Academy of Medical Sciences and Sichuan Provincial People's Hospital, Chengdu, China

[7]Discipline of Information & Communication Technology, University of Tasmania, TAS, Australia

***Corresponding Author:** Prof. Dr. Peng Xu
Address: No.2006, Xiyuan Ave, West Hi-Tech Zone, Chengdu, Sichuan, China, 611731.
Tel: +86-028-83206978, Fax: 86-028-83206978;
E-mail: xupeng@uestc.edu.cn

Abstract

Objective. Exploring the temporal variability in spatial topology during the resting state attracts growing interest and becomes increasingly useful to tackle the cognitive process of brain networks. In particular, the temporal brain dynamics during the resting state may be delineated and quantified aligning with cognitive performance, but few studies investigated the temporal variability in the electroencephalogram (EEG) network as well as its relationship with cognitive performance. *Approach.* In this study, we proposed an EEG-based protocol to measure the nonlinear complexity of the dynamic resting-state network by applying the fuzzy entropy. To further validate its applicability, the fuzzy entropy was applied into simulated and two independent datasets (i.e., decision-making and P300). *Main results.* The simulation study first proved that compared to the existing methods, this approach could not only exactly capture the pattern dynamics in time series but also overcame the magnitude effect of time series. Concerning the two EEG datasets, the flexible and robust network architectures of the brain cortex at rest were identified and distributed at the bilateral temporal lobe and frontal/occipital lobe, respectively, whose variability metrics were found to accurately classify different groups. Moreover, the temporal variability of resting-state network property was also either positively or negatively related to individual cognitive performance. *Significance.* This outcome suggested the potential of fuzzy entropy for evaluating the temporal variability of the dynamic resting-state brain networks, and the fuzzy entropy is also helpful for uncovering the fluctuating network variability that accounts for the individual decision differences.

Keywords: Fuzzy entropy, Resting-state EEG, Network variability, Decision-making

1. Introduction

Electroencephalogram (EEG) directly reflecting the neural electrical activity, is dynamic and varies across time scales. As one of the most complex dynamic systems, the brain constantly constructs and updates the internal network models to anticipate and plan future adaptive behaviors (Braun *et al* 2015, Jiang *et al* 2019). The brain at rest is also active both physiologically and psychologically (Damoiseaux *et al* 2006, Mantini *et al* 2007), and related resting-state brain activity has been proved to serve as the neural basis underlying the potential task information processing (Wang *et al* 2019, Hearne *et al* 2017). Just as illustrated, related brain networks at rest can effectively characterize the intrinsic allocation of the brain resources (Falahpour *et al* 2018, Northoff *et al* 2010) and also help predict the individual performance during the following tasks (Li *et al* 2013a, Zhou *et al* 2012), as well as individual mental state (Tian *et al* 2017a). For example, both the resting-state network topologies and properties were found to be positively related to the P300 amplitudes that were evoked by the target stimuli during the oddball tasks (Li *et al* 2015). At its initial stage, the resting-state network is believed to be stable, while plenty of recent studies find that the brain network at rest also fluctuates over time (Betzel *et al* 2016, Yu *et al* 2015, Garrett *et al* 2011). To quantitatively capture the fluctuating brain variability, the sliding window is usually used, which measures the time series of the dynamic functional connectivity. Several methods are then developed to explore the fluctuating variability across the time scales, which includes the variance of dynamic network connectivity, the network dissimilarity over time, and non-linear test statistics (Sun *et al* 2019, Zalesky *et al* 2014, Sakoglu *et al* 2010). For example, the network dissimilarity illustrated that better individual verbal creativity correlates with higher temporal variability in resting-state functional connectivity among multiple regions, such as the lateral prefrontal cortex, parahippocampal gyrus, and precuneus (Sun *et al* 2019).

Theoretically, the more diverse the fluctuating patterns of a given time series are, the high complexity the corresponding time series will be, that is, the signal is more irregular. The temporal complexity of a system can index its fluctuating dynamics; for a given signal, entropy has been widely used to quantify the corresponding signal complexity. The entropy can nonlinearly measure how complex (i.e., level of irregularity) the physiological signal will be (Gao *et al* 2015) and thus is proportional to signal irregularity; the larger the entropy, the more irregular the signal. Therefore, measuring the signal entropy in the temporal domain will deepen our knowledge of brain dynamics (Abasolo *et al* 2006, Tian *et al* 2019, Tian *et al* 2017b) and provide the possibility to quantitatively evaluate the temporal complexity of the physiological system (Takahashi *et al* 2010). Fuzziness is an alternative approach used when describing the uncertainty of a time series and the corresponding fuzzy entropy measurement has been proved to have great potential for avoiding the undesirable boundary effect (a sharp distinction of the boundary), compared to the other entropies, such as approximate entropy and sample entropy (Chen *et al* 2009); in the meantime, stronger relative consistency and less dependence on data length of the Fuzzy entropy further facilitate its application in evaluating the signal complexity (Li *et al* 2013b, Xie *et al* 2010). Therefore, the fuzzy entropy can effectively guarantee the estimated signal metrics to vary smoothly and continuously with similarity tolerance. Recently, fuzzy entropy has been widely applied to measure the complexity of both EEG and electromyogram (Cao *et al* 2018, Cao and Lin 2018, Masulli *et al* 2020), as well as investigating brain diseases, such as epileptic seizure (Cao *et al* 2020,

Xiang *et al* 2015), schizophrenia (Yang *et al* 2015), and Alzheimer's Disease (AD) (Simons *et al* 2018). For example, when using the network-based Takagi-Sugeno-Kanga fuzzy classifiers to identify the AD patients, related network metrics under eyes-closed and eyes-open conditions achieved relatively high accuracies of 97.3% and 94.78%, respectively (Yu *et al* 2020).

However, most of the current approaches mainly focus on the amplitude stationarity of brain networks to measure the dynamics of the temporal network variability (Zalesky *et al* 2014, Hindriks *et al* 2016) but neglect the inherent fluctuating network patterns that are remarkably helpful for reflecting how the brain network fluctuates over time. As illustrated previously, the corresponding network patterns, such as the network topological alterations, could promote the classification among different conditions (Moon *et al* 2020, Pena-Gomez *et al* 2018). For example, Shirer and colleagues used the whole-brain connectivity patterns to decode subject-driven cognitive states and achieved an accuracy of 84% (Shirer *et al* 2012), and when using network topological alterations to accomplish the fatigue classification, Dimitrakopoulos and colleagues also achieve high accuracy of 92% for driving and 97% for psychomotor vigilance task (Dimitrakopoulos *et al* 2018). Moreover, corresponding network complexity has also been proved to have great potential for indexing the flexible and robust network architectures and reflecting how the brain could respond to cognitive stimuli (Sun *et al* 2019). To effectively explore the mechanism underlying the cognitive process in the brain, exactly capturing the fluctuating network patterns, e.g., flexible and robust architectures, will play an important role and help reflect to which degree the brain can respond to the upcoming task. Therefore, contrary to the traditional methods that measure the amplitude stationarity (Zalesky *et al* 2014, Hindriks *et al* 2016), our current work mainly focused on exploring the fluctuating temporal patterns of the time-varying resting-state brain networks, to uncover the potential fuzzy evidence underlying the decision differences between different individuals.

Herein, we assumed that the fluctuating temporal variability in resting-state networks can be effectively captured by fuzzy entropy, and related variability metrics do closely relate to individual cognitive behaviors. To validate this approach, besides a simulation study, the proposed metric was further applied to the real dataset of decision-making that was collected from adolescents and adults when they responded to the unfair offers. As a high-level cognitive process, decision-making involves a wide range of complex behaviors (Cecchetto *et al* 2017, Preuss *et al* 2016) and is attributed to the functional interactions of those spatially separated but functionally linked brain regions (Si *et al* 2020a, Si *et al* 2019b). Understanding the neural substrates of decision-making helps establish effective artificial intelligence and brain-computer interface (BCI) as well, where the decision-making is of great importance for individuals (Long *et al* 2012, Li *et al* 2013c). The theories of (culture-specific) socialization (Hoffmann and Tee 2006, Marchetti *et al* 2019) and childhood development (Castelli *et al* 2010, Castelli *et al* 2014, Guroglu *et al* 2009) demonstrate that the preference for fairness increases with age, and adolescents usually make relatively larger acceptances than the adults, as they preferred the outcome even under unfair conditions (Sutter 2007, Si *et al* 2020b).

Moreover, P300 has also been demonstrated to be attributed to the functional interactions of multiple regions in the brain, including the middle frontal gyrus, insula, and thalamus, etc (Li *et al* 2020, Bledowski *et al* 2004), and could effectively index various cognitive functions, such as attention allocations and working memory (Polich 2007). As one of the

electrophysiological biomarkers, P300 has been widely used to evaluate the subject's capacity during tasks (Wang *et al* 2015a), as well as classify different individual groups (Turetsky *et al* 2015). Uncovering related neural mechanism also helps deepen our understanding of P300 and contributes to its future applications in multiple aspects, such as BCI and clinical diseases, etc. Following decision-making, to further validate the applicability of the fuzzy entropy in capturing the fluctuating temporal variability of resting-state networks, an independent P300 resting-state EEG dataset was also investigated by adopting the same analytical protocols.

2. Materials and methods

2.1. *Fuzzy entropy of the dynamic networks*

Fuzzy entropy can effectively evaluate signal complexity, especially for the short time series contaminated by noise (Chen et al 2009), and is insensitive to disturbance but sensitive to the fluctuations of related information content (Acharya et al 2015). A higher value of fuzzy entropy represents the larger temporal variability in time series.

Assuming there are N networks, the time series for each network edge can be termed as X_i ($1 \le i \le N$) whose value varies from 0 to 1, which is formed as follows;

$$X_i^m = \{u(i), u(i+1), \ldots, u(i+m-1)\} - u_0(i), i = 1, \ldots, N-m+1 \quad (1)$$

where X_i^{m} represents m consecutive u values (i.e., coherence value) at i-th network point, which is generalized by removing the baseline $u_0(i) = m^{-1} \sum_{j=0}^{m-1} u(i+j)$.

Given r, calculating the similarity degree D_{ij}^m between X_i^{m} and its neighboring vector X_j^{m}, which is formulized as follow;

$$D_{ij}^m = \mu\left(d_{ij}^m, r\right) \quad (2)$$

where d_{ij}^m is the maximum absolute difference of the corresponding scalar components of X_i^{m} and X_j^{m}. For each vector X_i^{m} (i = 1, 2, …, N-m+1), by averaging all similarity degree, D_{ij}^m, of its neighboring vectors X_j^{m} (i = 1, 2, …, N-m+1, and $j \neq i$), we then get

$$f_i^m(r) = (N-m-1)^{-1} \sum_{j=1, j \neq i}^{N-m} D_{ij}^m \quad (3)$$

Relying on $\jmath^m(r) = (N-m)^{-1} \sum_{i=1}^{N-m} f_i^m(r)$ and $\jmath^{m+1}(r) = (N-m)^{-1} \sum_{i=1}^{N-m} f_i^{m+1}(r)$, we then define the *FuzzEn*(m, r) of the time series X_i ($1 \le i \le N$) as follow;

$$FuzzEn(m, r) = \lim_{N \to \infty} \left[\ln \jmath^m(r) - \ln \jmath^{m+1}(r)\right] \quad (4)$$

which can be estimated by the statistic,

$$FuzzEn(m, r, N) = \ln \jmath^m(r) - \ln \jmath^{m+1}(r) \quad (5)$$

where m denotes the length of the compared window, r denotes the width of the boundary for similarity measurement, and N denotes the length of related time series to be analyzed. Particularly, large m guarantees a more detailed reconstruction of the dynamic process, but an

overlarge m might lead to information loss (Pincus and Goldberger 1994). Just as proposed in the previous study (Chen *et al* 2007), m was determined to be 2. In the meantime, rather small r brings the noise, but too large r might also result in information loss, which is, therefore, set to 0.2 multiplied by the standard deviation of the time series in this study.

2.2. *Validation on simulated data*

To evaluate whether the proposed fuzzy entropy-based analysis could capture the fluctuating temporal variability in the dynamic resting-state networks, we first simulated the dynamic networks that varied across time scales, whose network edge strengths vary over time. To fulfill this aim, the $MIX(p)$ with varying parameter p values ($0 \le p \le 1$) was used to formulate the network edges between two nodes (Pincus 1991, Pincus 1995), whose time series had varying complexity. The $MIX(p)$ is a series of sampling processes for the stacking waves of sines and cosines at $p = 0$ or independent uniform random variables at $p = 1$. Meanwhile, to test if the proposed method was sensitive to the magnitude of the signal, the varying magnitudes were also simulated with another parameter i, as i was set as 0.1, 0.5, 1, 5, and 10. Herein, for each time point j in the simulated time series, we first defined the $MIX^{(i)}(p)$ as follow;

$$MIX^{(i)}(p)_j = i\left(1 - Z_j\right)X_j + Z_j Y_j - H_j \tag{6}$$

where X_j represents the stochastic and deterministic signal formed by the sine and cosine signal, and $X_j = \frac{7}{100}\sin\left(\frac{\pi}{50}j + \frac{p\pi}{6}\right) + \frac{3}{100}\sin\left(\frac{\pi}{500}j + \frac{p\pi}{6}\right) + \frac{1}{25}\cos\left(\frac{9\pi}{1000}j\right) + \frac{1}{20}\cos\left(\frac{\pi}{125}j\right) + 0.8$, Y_j represents a family of independent identically distributed real random variables, with uniform density in the interval [0, 0.3], Z_j represents the random variable, where $Z_j = 1$ with probability p, $Z_j = 0$ with probability 1 - p, and H_j represents a discrete step function.

As the p-value increases, the time process becomes intuitively more irregular, that is, a larger p denotes the higher complexity of the signal (i.e., the corresponding edge has more complicated patterns). In this study, we simulated a weighted network with 5 nodes (Fig. 3a), in which each edge had varied predefined complexity with the p-value being selected within a range of [0.1, 0.5]. With the predefined signal complexity determined by p, the five time-varying edges were simulated between pairs of nodes (nodes A and C, nodes B and D, nodes C and D, nodes C and E, and nodes D and E) in Fig. 3a.

In this study, apart from the fuzzy entropy, other traditional approaches, such as variance (Sakoglu *et al* 2010) and non-linear test statistic (Zalesky *et al* 2014), were also used to measure related fluctuating temporal complexity of these edges in our predefined 5-nodes network. Furthermore, to acquire a robust simulated result, the $MIX^{(i)}(p)$ and the estimation of fluctuating temporal complexity were repeated 1,000 times. Finally, the averaging across 1000 times is used to evaluate and compare the capacity of different approaches in measuring the fluctuating temporal variability of the brain networks.

2.3. *Validation on decision-making data*

2.3.1. Participants. The experiment protocol was approved by the Institution Research Ethics Board of the University of Electronic Science and Technology of China (UESTC) and was conducted following the Declaration of Helsinki. Two independent groups of participants (i.e., postgraduate and

junior high school students) were recruited and paid for their efforts to take part in this study at UESTC. Before they joined our experiments, participants were told about the experimental details and then read and signed their names on the written informed consent. Eighteen postgraduate students (5 females, age range of 21-24 years, and mean 23.45 years) from the UESTC and 22 junior high school students (10 females, age range of 14-16 years, and mean 14.59 years) from The Experimental High School Attached To UESTC were included in this study. None of the participants had a history of neurological or psychiatric disorders and were not currently using any psychoactive medications. All of them had normal or correct-to-normal visual acuity.

2.3.2. Experimental protocols. In the ultimatum game (UG) task, the participant acted as a responder who would decide to accept or reject an offer given by the proposer (i.e., the computer itself). If he or she accepted the offer, both players (i.e., responder and proposer) received the money according to the splits; in case of rejecting it, they would not earn anything. When playing with the computer game, participants were advised to play this game with another participant in a separate room. Experiments were performed in a quiet, dimly lightroom. Participants were first instructed to take a deep breath to adapt to the experimental environment. Before the UG task, 5 minutes of eyes-closed resting-state EEG datasets were recorded, which was followed by an 8.5 min UG task.

Fig. 1 illustrates the timeline of the UG task. In the UG task, the sum of splits was ¥ 10; meanwhile, three categories were included, i.e., the fair offer (¥ 5 vs. ¥ 5), moderately unfair offer (¥ 3 vs. ¥ 7), and extremely unfair offer (¥ 1 vs. ¥ 9). A total of 90 offers, 30 offers per condition, were included in the UG task. Each UG trial began with an 800 ms thin cross. Then, a screen with ¥ 10 appeared and lasted 500 ms, which was followed by a 1,000 ms black screen. Thereafter, a split offer was presented, at the same time, participants need to decide to reject ("3") or accept ("1") the offer by pressing the button on the standard keyboard. Followed by their choice, the feedback appeared to inform their received money on that trial, as well as the cumulative winnings of participants. The decision and feedback would keep 2,700 ms in total.

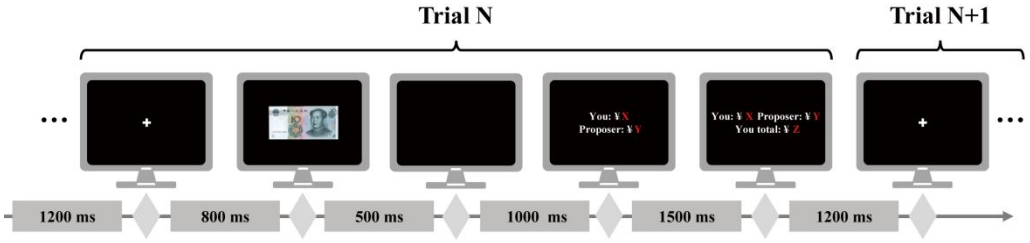

Fig. 1. The timeline of a UG task trial.

2.3.3. EEG recording. Participants were seated in an electrically shielded and light-attenuated room. The 64-channels resting-state EEG datasets were recorded by using the ASA-Lab Amplifier (ANT Neuro), and the 64 Ag/AgCl electrodes were positioned in compliance with the extended 10-20 international electrode system. During the data recording, the EEGs were digitized with a sampling rate of 500 Hz, and online bandpass filtered within the frequency range of [0.05 Hz, 70 Hz]. The electrodes of CPz and AFz served as the reference and ground, respectively. The electrooculogram was recorded from one channel located at the above side of the left eye to monitor eye movements. For all electrodes, the impedance was consistently below 5 KΩ throughout the experiment.

2.3.4. Fuzzy entropy of resting-state EEG network. In fact, these decision-making datasets had been reported in our previous study (Si *et al* 2019b), since our present study focused on investigating the resting-state network variability, only the resting-state EEG datasets were used here. Although the potential mechanism of the decision-making differences had been explored in previous studies from the perspective of ERP and power spectra, etc (Villafaina et al 2019, Kim et al 2021), decision-making is proved to be attributed to the functional interactions of those spatially separated but functionally coupled regions (Si et al 2020a, Si et al 2019b). Moreover, related fluctuating temporal patterns in decision networks are still been left unveiled, although the corresponding network complexity has also been proved to help identify the temporal variability in network architecture and index how the brain responds to cognitive stimuli (Sun *et al* 2019, Zalesky *et al* 2014). Therefore, when exploring the potential mechanism underlying the decision-making, identifying the corresponding temporal variability in decision network architectures, e.g., flexible and robust network patterns, will be of great importance and also help index to which degree the brain could respond to the unfair conditions. The analytical protocols for exploring the brain variability in dynamic resting-state networks were first displayed in Fig. 2, and the detailed procedures were further depicted as follows.

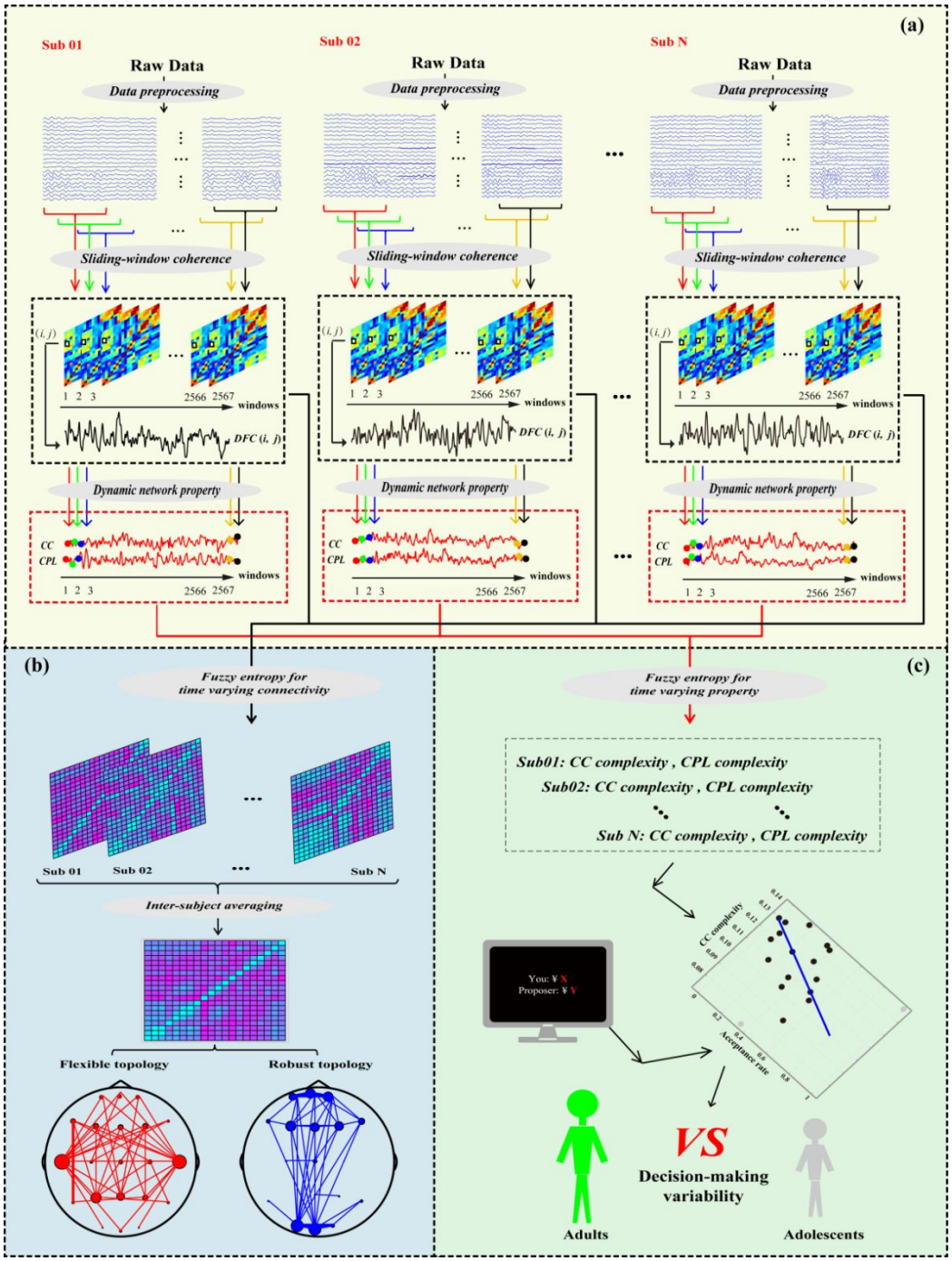

Fig. 2. Analytical protocols of the temporal variability in the resting-state EEG network. (a) Dynamic resting-state network construction, (b) The complexity of the dynamic resting-state network topologies, and (c) The temporal complexity of the dynamic resting-state network properties and Pearson's correlation analysis between network properties complexity and UG task behaviors. DFC denotes dynamic functional connectivity.

Before exploring related brain variability in these time-varying resting-state networks, the resting-state EEG datasets were first preprocessed. Concretely, to remove the artifacts, the resting-state EEG datasets were first referenced to a neutral reference of Reference Electrode Standardization Technique (REST) (Dong *et al* 2017, Yao 2001), and then offline bandpass

filtered within the frequency range of [0.5 Hz, 30 Hz]. Thereafter, the independent component analysis (ICA) was adopted to remove residual artifacts (He *et al* 2005) that still contaminate EEG data by removing related artifact components.

The brain network is typically modeled by graph theory and includes a collection of nodes and edges. The EEG electrodes were considered as network nodes, and the synchronized strengths between pairwise electrodes estimated by coherence were set as network edges. Due to the effect of volume conduction, the nearby electrodes acquire similar contributions from cortical sources and thus capture a similar activity. In our present study, to reduce the effect of volume conduction, following the procedure in related studies (Qin *et al* 2010, Huang *et al* 2017), 21 canonical electrodes (i.e., FP1/z/2, F7/3/z/4/8, T7/8, C3/z/4, P7/3/z/4/8, and O1/z/2) out of the 64 channels in the 10-20 system were used to construct the resting-state network. Theoretically, coherence can effectively measure the synchronized neuronal assembly at any given frequency bin f between pairwise signals, $x(t)$ and $y(t)$, and is usually formulated as,

$$C_{xy}(f) = \left|R_{xy}(f)\right|^2 = \frac{\left|P_{xy}(f)\right|^2}{P_{xx}(f)P_{yy}(f)} \tag{7}$$

where $C_{xy}(f)$ and $R_{xy}(f)$ represent the estimated coherence value and the complex correlation coefficient between $x(t)$ and $y(t)$ at frequency bin f, respectively. At per frequency bin f, $P_{xy}(f)$ represents the cross-spectrum between $x(t)$ and $y(t)$, $P_{xx}(f)$ and $P_{yy}(f)$ represent the auto-spectrum of $x(t)$ and $y(t)$, respectively. These measurements of spectral densities were calculated from the Fast Fourier Transform. For each frequency bin f, the $C_{xy}(f)$ is calculated by squaring the magnitude of the complex correlation coefficient R between $x(t)$ and $y(t)$, which returns a real value within the range of [0, 1]. Since this study focused on the fluctuating variability of brain activity at rest, we thus concentrated on the alpha band ([8, 13] Hz) to construct the corresponding resting-state network.

In our present study, the time-resolved resting-state network was calculated by using a 5-s sliding-window approach with an overlapping of 98% that can provide 100 ms temporal resolution for dynamic networks, which resulted in the time-varying networks varied across time scales. Based on the time-varying resting-state networks, a time series would be obtained for each network edge, and when the corresponding variability is calculated for each edge by the fuzzy entropy, the variability of network topology could be achieved, which can reflect how stable each network edge is (Fig. 2a). After the above procedure, each subject will have a network topology complexity and a network property complexity. For network topological complexity, it can reveal the distribution of spatial topological variability clearly, which can reflect the robust or flexible spatial pattern. Finally, by grand-averaging across subjects, the network topology complexity accounting for all subjects could be achieved (Fig. 2b).

Thereafter, a threshold strategy was used in identifying the fluctuating temporal patterns in resting-state networks; concretely, the 20% network edges with the largest and smallest fuzzy entropy were adopted to index the flexible and robust network architectures for both groups, respectively. However, when calculating related resting-state network properties, including nodal degree (*ND*), clustering coefficients (*CC*), global efficiency (*GE*), local efficiency (*LE*), and characteristic path length (*CPL*) (Rubinov and Sporns 2010), the fully-connected weighted adjacency matrices without any thresholding were used. Theoretically, the *ND* sums

all edge strengths connecting one network node and reflects the importance of this node in a given network, the *CC* and *LE* index the functional segregation of a given network and both reflect the capacity for specialized processing within densely interconnected regions, while the *CPL* and *GE* measure the functional integration and index the ability to rapidly combine specialized information from distributed regions. Here, based on the fully-connected weighted adjacency matrix per subject, let C_{ij} be the synchronized strength between nodes i and j estimated by coherence, d_{ij} represents the shortest weighted path length, N represents the number of all nodes, and Θ represents the set of network nodes. The *ND*, *CC, GE*, *LE*, and *CPL* were then formulized as follows.

$$ND_i = \sum_{j \in \Theta} C_{ij} \tag{8}$$

$$CC = \frac{1}{N} \sum_{i \in \Theta} \frac{\sum_{j,l \in \Theta} \left(C_{ij} C_{il} C_{jl} \right)^{1/3}}{\sum_{j \in \Theta} C_{ij} \left(\sum_{j \in \Theta} C_{ij} - 1 \right)} \tag{9}$$

$$CPL = \frac{1}{N} \sum_{i \in \Theta} \frac{\sum_{j \in \Theta, j \neq i} d_{ij}}{N-1} \tag{10}$$

$$GE = \frac{1}{N} \sum_{i \in \Theta} \frac{\sum_{j \in \Psi, j \neq i} \left(d_{ij} \right)^{-1}}{N-1} \tag{11}$$

$$LE = \frac{1}{N} \sum_{i \in \Theta} \frac{\sum_{j,h \in \Theta, j \neq i} \left(w_{ij} w_{ih} \left[d_{jh} \left(\Theta_i \right) \right]^{-1} \right)^{1/3}}{\sum_{j \in \Theta} w_{ij} \left(\sum_{j \in \Theta} w_{ij} - 1 \right)} \tag{12}$$

Since the small-worldness has been widely used in brain networks to investigate the human cognitive process (Bassett and Bullmore 2017), as well as measuring the capacity of stimuli modulation, such as acupuncture (Yu *et al* 2018), in our present study, the small-worldness is also adopted as one of the variability metrics to measure the resting-state brain networks. Theoretically, small-worldness is quantified by the *CPL* and *CC* and reflects the regional specialization and the information transfer efficiency in the brain. Before calculating the small-worldness, the *CC* and *CPL* of the constructed EEG networks (i.e., CC_t and CPL_t) are normalized by dividing by the value for the same variable calculated for a randomly rewired null model, which are then termed as γ and λ, respectively. Here, the *CC* and *CPL* of the random network (i.e., CC_r and CPL_r) are the averages of the values calculated from 1000 randomly rewired null models.

$$\gamma = \frac{CC_t}{CC_r} \tag{13}$$

$$\lambda = \frac{CPL_t}{CPL_r} \tag{14}$$

Finally, the small-worldness, *sw*, is given by a ratio of the normalized *CC*, γ, to the normalized *CPL*, λ, as,

$$sw = \frac{\gamma}{\lambda} \tag{15}$$

Herein, by using the brain connectivity toolbox (BCT), we quantitatively calculated the corresponding network properties for each dynamic network, resulting in the dynamic resting-state network properties (i.e., *CC*, *CPL*, *GE*, *LE*, and small-worldness) that varied across time. Then, the temporal variability of these parameters could also be quantitatively measured by the fuzzy entropy, which reflected the fluctuating complexity in the properties time series (Yu *et al* 2015, Thompson *et al* 2017) (Fig. 2a).

Although, the acceptance rate (AR) varies across subjects but relatively keeps stable intra-subject, and is thus used to characterize the individual task behavior during tasks (Wang *et al* 2017). Besides, the cumulative winning (CW) is also regarded as a direct measurement of task behavior during the UG task. We then obtained the AR of combining the extremely and moderately unfairness conditions, as well as the CW throughout the UG task.

As proved in previous studies, the corresponding resting-state brain network has great potential for facilitating the prediction of individual performance during the following tasks (Li *et al* 2013a, Zhou *et al* 2012), for example, when using related resting-state network properties to predict individual acceptance rate during the UG task, the predicted rates were also found to be significantly correlated with the actual rates (Si *et al* 2019a). In our present study, concerning the resting-state network properties complexity, the correlation analysis was further implemented to investigate any possible relationships between resting-state network properties complexity and individual decision behavior (AR and CW, Fig. 2c). To obtain the robust representative knowledge underlying the variability in decision-making between the two groups, the outliers were marked relying on the relationships between network property variability and task behaviors. In detail, participants with the 10% largest Malahanobis distances (Zhang *et al* 2015) to the data center were considered as the outliers and then excluded from the correlation analysis.

3. Results

3.1. Simulated network

In this simulation study, the complexity of each network edge measured by the fuzzy entropy was first displayed in Fig. 3b, which demonstrated a similar tendency with the predefined complexity per time series (Fig. 3a), for example, the edge D-E showed the largest complexity in both Fig. 3a and 3b. However, as shown in Figs. 3c and 3d, the other two methods inversely presented the largest complexity of edge A-C that had the smallest complexity in the current simulation, which unfortunately estimated the opposite tendency of the temporal complexity.

Moreover, the variance and non-linear test statistic were found to be indeed sensitive to the magnitude of the signal. Along with the increased magnitude, both methods estimated the increased signal complexity, which revealed $MIX^{(10)}(p) > MIX^{(5)}(p) > MIX^{(1)}(p) > MIX^{(0.5)}(p) > MIX^{(0.1)}(p)$ per complexity case (Fig. 3f and 3g). In contrast, the fuzzy entropy was not affected by the increased magnitude (Fig. 3e), as the same complexity was accurately estimated by the fuzzy entropy for all the five magnitude cases.

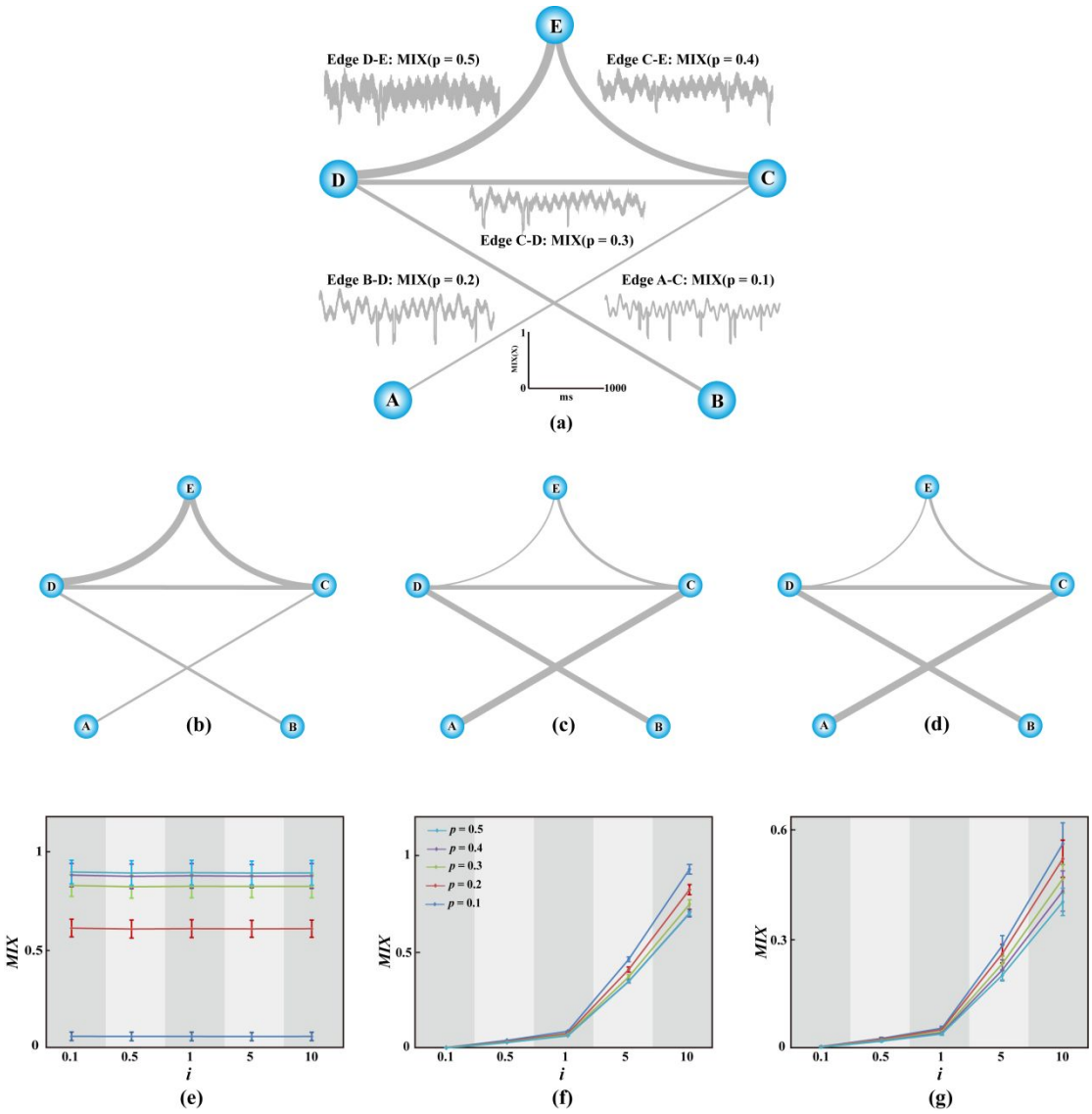

Fig. 3. Simulated 5-nodes network with $MIX^{(i)}(p)$ (p = 0.1, 0.2, 0.3, 0.4, and 0.5) (a) and the estimated temporal complexity of the network edge by the fuzzy entropy (b), variance (c), and non-linear test statistic (d). In subfigures (b - d), the width of the solid line denotes the predefined or estimated temporal complexity of a given edge. Subfigures (e - g) denote the varied temporal complexity of the network edge estimated by the fuzzy entropy (e), variance (f), and non-linear test statistic (g) for all the five magnitude cases.

3.2. Variability in decision-making network topology

Figs. 4a and 4b display the 20% network edges with the largest (i.e., flexible) and smallest (i.e., robust) fuzzy entropy, respectively. Specifically, the flexible architectures of both postgraduate and junior high school students were consistently distributed at the bilateral temporal lobe (Fig. 4a), and the nodes were further printed with deep red color (i.e., high entropy) as shown in Fig. 4c. By contrast, for both groups, Fig. 4b illustrates a similarly robust architecture that seemed to be a resting-state default mode network (DMN), where the 20% edges with the smallest fuzzy entropy linked the frontal and occipital lobe.

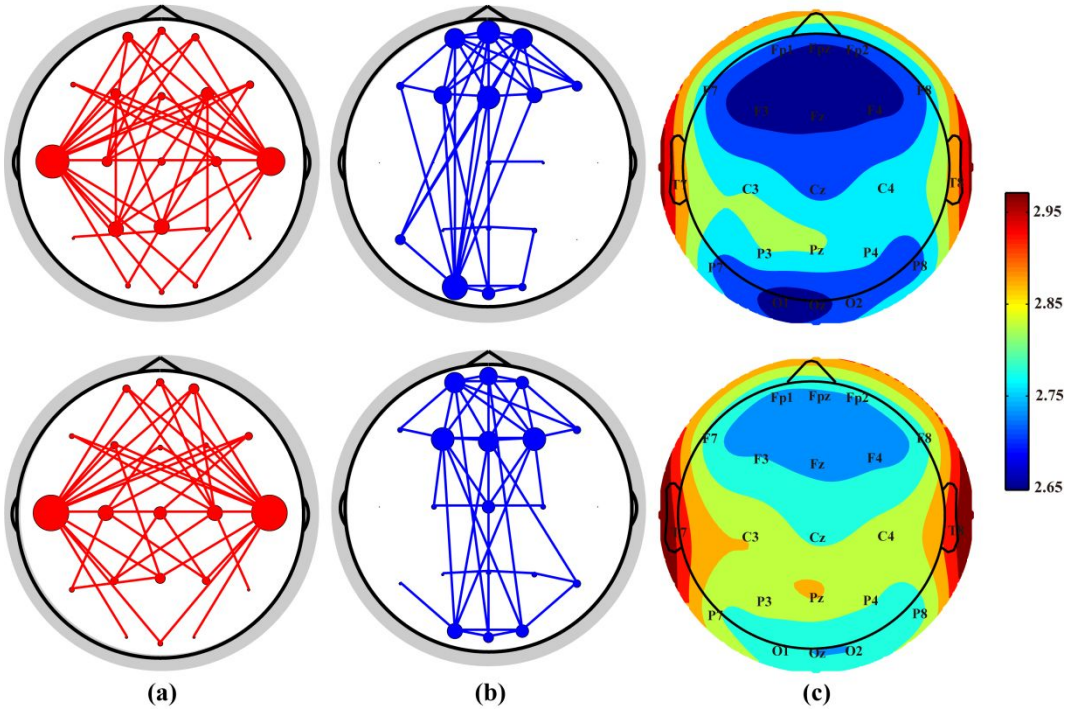

Fig. 4. Scalp topologies with the 20% largest and smallest fuzzy entropy for both groups. (a) Flexible architecture, (b) Robust architecture, and (c) Nodal degree distribution. The first and second row denotes the postgraduate students and junior high school students, respectively. In subfigures (a, b), the size of each electrode is proportional to its binary degree in the 20% largest and smallest network, respectively.

3.3. The relationships between network variability and decision behaviors

Thereafter, for both flexible and robust resting-state network architectures displayed in Fig. 4, the weights of flexible and robust network edges were averaged separately to achieve the averaged flexible and robust variability metrics per student in both postgraduates and junior high school groups. Thereafter, the averaged flexible and robust variability metrics of both groups were statistically compared separately, and as displayed in Fig. 5, we found the flexible metrics of postgraduate students were significantly larger than that of junior high school students ($p < 0.05$), while the robust metrics between two groups were opposite to the flexible metrics ($p < 0.05$).

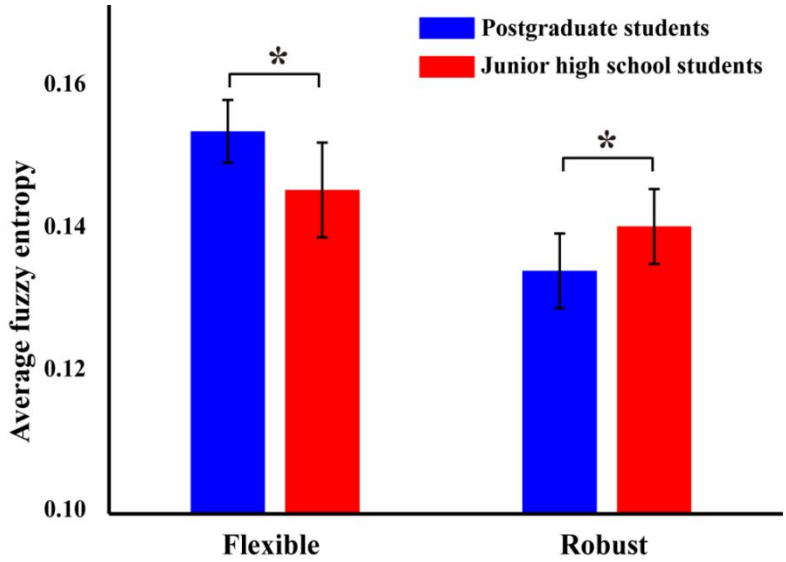

Fig. 5. The differences in the flexible and robust network variability metrics between postgraduate students and junior high school students. The red-filled bars denote the junior high school students, the blue-filled bars denote the postgraduate students, and the symbol * denotes $p < 0.05$.

Meanwhile, based on these flexible and robust variability metrics per student, the classification of postgraduate students versus junior high school students was further performed by adopting the leave-one-out cross-validation (LOOCV) strategy (Zeng *et al* 2012). Herein, considering m (m = 40 of both postgraduates and junior high school students) samples, in each LOOCV procedure, m-1 subjects were used to training the linear discriminant analysis (LDA) classifier, and the remaining 1 sample was used for testing until all subjects were served as testing for one time. After the LOOCV was finished, the corresponding classification accuracy would be then reported. Here, Fig. 6 displays the scatterplot of flexible and robust variability metrics, which indicated that these metrics could accurately classify both groups, and indeed, the LDA could achieve an accuracy of 92.50% when classifying these subjects by using the variability metrics proposed in this study.

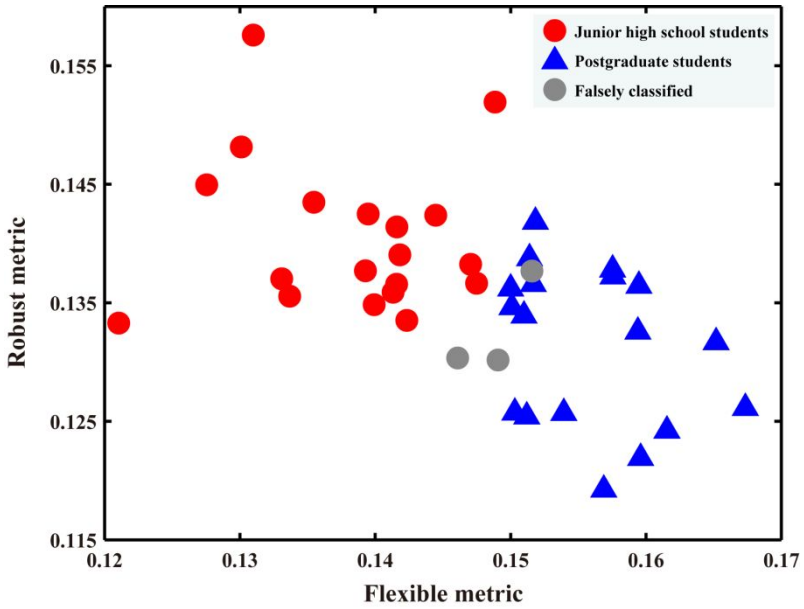

Fig. 6. The scatterplot of flexible and robust network variability metrics. The red-filled circles denote the junior high school students, the blue-filled triangles denote the postgraduates, and the grey-filled circles denote the falsely classified students.

Finally, the potential relationships between individual decision behaviors and network variability for postgraduate students and junior high school students were investigated, and the opposite tendencies of both variables between the two independent groups were displayed in Figs. 7 to 10. Concretely, for postgraduate students (Figs. 7 and 8), Fig. 7 showed that the individual decision AR was marginally significantly negative-correlated with the *CC* (r = -0.479, p = 0.060), *GE* (r = -0.489, p = 0.055), *LE* (r = -0.472, p = 0.065), *CPL* (r = -0.435, p = 0.092; CW:), and small-worldness (r = -0.529, p = 0.035). Concerning the CW displayed in Fig. 8, similar tendency was found, as the CW also illustrated the significantly negative relationship with the *CC* (r = -0.488, p = 0.055), *GE* (r = -0.542, p = 0.030), *LE* (r = -0.522, p = 0.038), *CPL* (r = -0.522, p = 0.038), and small-worldness (r = -0.610, p = 0.012).

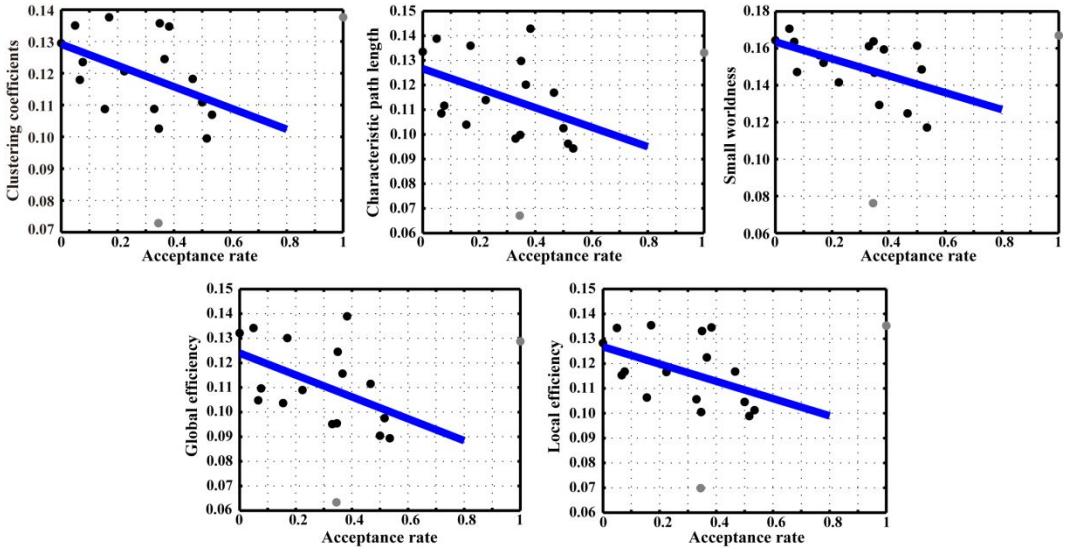

Fig. 7. The relationship between resting-state network variability metrics and the acceptance

rate for postgraduate students. In each subfigure, the blue lines denote the fitted linear trend between two variables, the black and grey filled circles denote the included and outlier subjects, respectively.

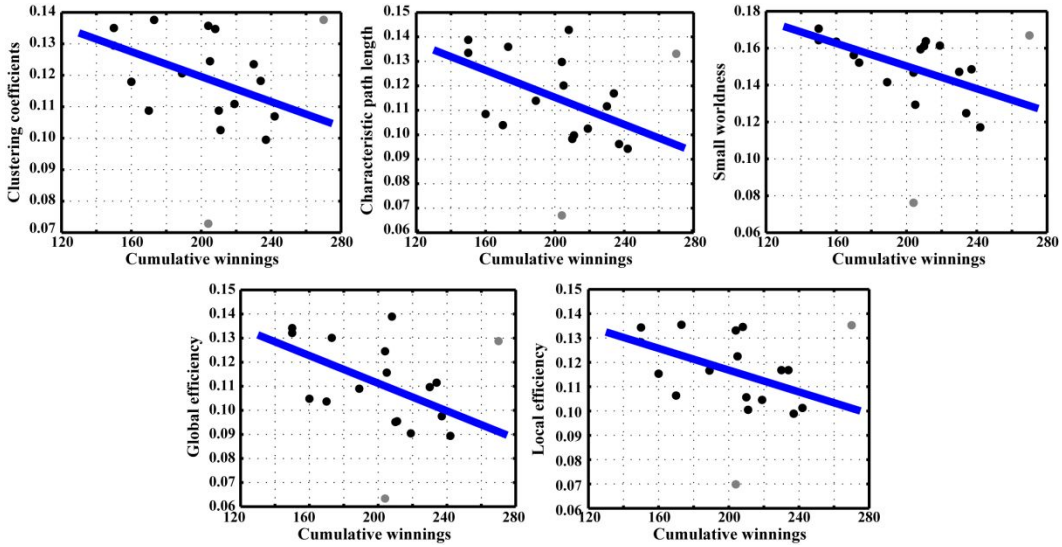

Fig. 8. The relationships between resting-state network variability metrics and the cumulative winnings for postgraduate students. In each subfigure, the blue lines denote the fitted linear trend between two variables; the black- and grey-filled circles denote the included and outlier subjects, respectively.

By contrast, the corresponding relationships between resting-state network variability metrics and individual decision behaviors for the junior high school students were further displayed in Figs. 9 and 10. In detail, as illustrated in Fig. 9, the *CC* (r = 0.545, p = 0.013), *GE* (r = 0.419, p = 0.066), *LE* (r = 0.516, p = 0.020), *CPL* (r = 0.506, p = 0.023), and small-worldness (r = 0.512, p = 0.021) were found to be significantly and positively related to the decision AR in junior high school students. Concerning the CW in junior high school students, Fig. 10 eventually illustrated that the individual CW also showed the significantly positive relationships with the *CC* (r = 0.634, p = 0.003), *GE* (r = 0.500, p = 0.025), *LE* (r = 0.603, p = 0.005), *CPL* (r = 0.587, p = 0.007), and small-worldness (r = 0.512, p = 0.021) of their resting-state network variability.

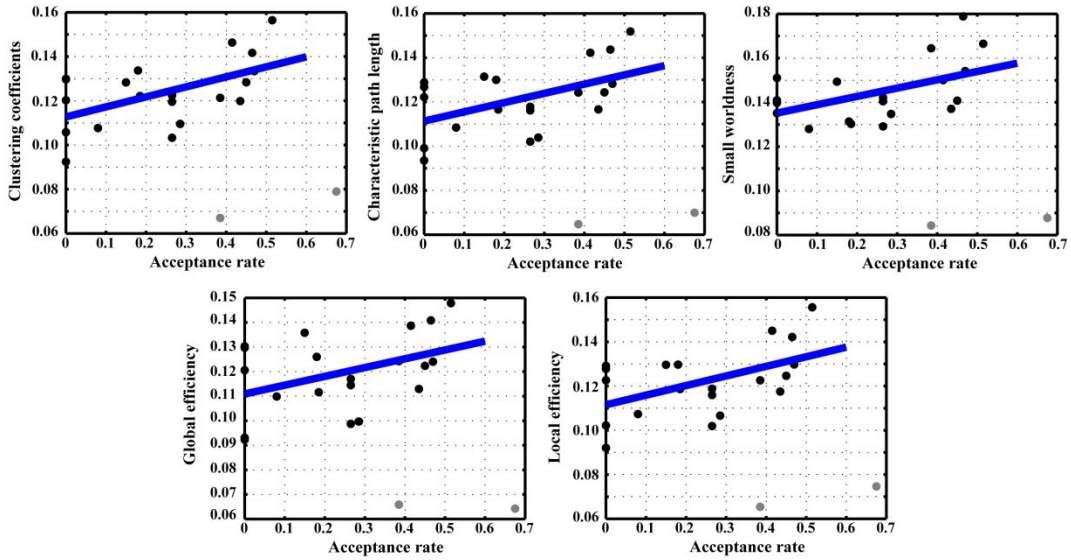

Fig. 9. The relationship between resting-state network variability metrics and the acceptance rate for junior high school students. In each subfigure, the blue lines denote the fitted linear trend between two variables, the black and grey filled circles denote the included and outlier subjects, respectively.

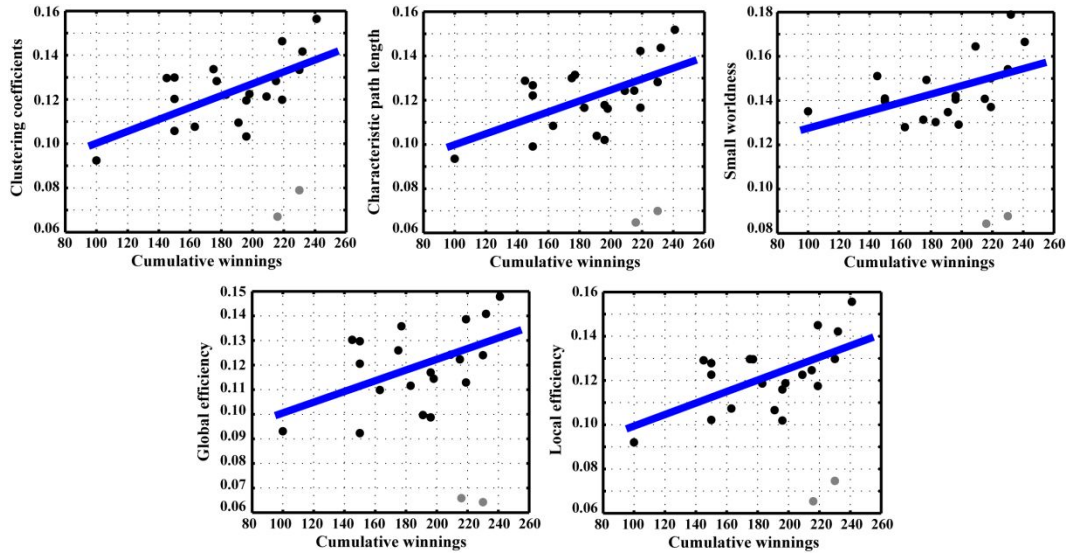

Fig. 10. The relationships between resting-state network variability metrics and the cumulative winnings for junior high school students. In each subfigure, the blue lines denote the fitted linear trend between two variables; the black and grey filled circles denote the included and outlier subjects, respectively.

4. Discussion

When referring to the time-resolved function connectivity, the network connectivity fluctuates in a transient time interval (Hutchison *et al* 2013), and these fluctuations are further found to be related to the modularity of brain network architecture (Pedersen *et al* 2018, Lurie *et al* 2018). Fluctuating temporal variability in network topology corresponds to the varied flexibility in the network architecture, and the flexibility of those edges is believed to effectively index the brain activity (Lurie *et al* 2018, Allen *et al* 2014). Meanwhile, the

corresponding temporal flexibility might be measured by the temporal complexity of time-varying functional connectivity in the brain (Pedersen *et al* 2018). The entropy is useful in addressing the randomness (irregularity) of a given system, and higher entropy always associates with higher randomness, as well as the larger complexity. In this study, we thereby used the fuzzy entropy (Chen *et al* 2007, Chen *et al* 2009) to evaluate the fluctuating temporal variability in time-varying resting-state networks and further investigated the possible relationship between the resting-state network variability and individual decision behaviors. In addition, to validate the applicability of fuzzy entropy in capturing the fluctuating temporal variability, we also recorded and further analyzed another independent resting-state EEG dataset before a P300 task by the independent amplifier (i.e., Symtop Instrument, Beijing, China), which also demonstrated the similar flexible and robust resting-state architecture (see APPENDIX).

Just as depicted above, during the simulation study, edge D-E was defined by $MIX(p = 0.5)$ and had the largest complexity; while edge A-C was defined by $MIX(p = 0.1)$ and had the smallest complexity. Fig. 3 demonstrates that in contrast to the other approaches, such as the variance and non-linear test statistic based on the median, only the fuzzy entropy could accurately estimate the network edge complexity in a predefined 5-nodes network. In this study, the fuzzy entropy presented the precise complexity order of the five edges as edge D-E > edge C-E > edge C-D > edge B-D > edge A-C; nevertheless, the remaining approaches incorrectly identified the opposite tendency among the five edges. In fact, unlike fuzzy entropy, both methods are more concerned about capturing the fluctuation of signal magnitude (Dionisio *et al* 2007), while the fluctuating network pattern is more meaningful to uncover the neural basis of physiological signals. Under some specific situations, they will fail in describing the temporal complexity and even present the opposite tendency. On the contrary, fuzzy entropy is insensitive to the data magnitude (Fig. 3e) but depends more on the data distribution (Dionisio *et al* 2007), thus fuzzy entropy is more helpful to capture the dynamic fluctuations of network patterns. Therefore, we believed the simulation displayed in Fig. 3 effectively validated the applicability of fuzzy entropy in measuring the fluctuating temporal variability of the resting-state networks across time scales.

In essence, when the brain is at rest, along with participants' closing their eyes, the brain functions in an interoceptive state consisting of the imagination and sensory activity (Marx *et al* 2003, Marx *et al* 2004), at the same time, the intrinsic connectivity synchronization that relates to somatosensory (Fox *et al* 1987) and auditory network increases. For both groups, a highly flexible network architecture consistently experienced denser connectivity in the bilateral temporal lobe (Fig. 4a), which reflected that these regions overlapped with that activated by the interoceptive state under the eye-closed resting state. In essence, previous studies have demonstrated that the DMN is the core and inherent network in the brain (Shen 2015), and the dynamics of DMN may serve as the basis when switching between exteroceptive and interoceptive state (Wang *et al* 2015b). DMN relates to the individual internal process, self-generated thought, and mind wandering (Buckner and Vincent 2007, Anticevic *et al* 2012). In this study, for both groups, we consistently showed the DMN-like topology that indexes the robust network architecture, which was measured by fuzzy entropy (Fig. 4b). In essence, the flexibility in functional network connectivity closely relates to its complexity, an increase in edge flexibility corresponds to the higher signal complexity. An

interesting issue was that, although the network in a resting state indeed fluctuates in a transient time interval, we could still observe a steady DMN pattern connecting the frontal and occipital lobe. We assumed that this might be the reason why our previous study found a close relationship between the frontal-occipital long-range linkage and P300 (Li *et al* 2015), as well as other findings in related resting-state studies (Jann *et al* 2009, Prestel *et al* 2018).

Decision-making requires an effective evaluation of the current situation, which relies on effectively assessing external (i.e., monetary value) and internal factors (i.e., fairness) (Huerta and Kaas 1990). The decision-making in adults and adolescents is usually influenced by many factors including inhibitory control, learning, emotion, and social context (Gladwin *et al* 2011, Rubia *et al* 2000), and distinctive decision behaviors between the two groups have been found in our previous study (Si *et al* 2020b). While time-resolved investigation allows the fine-grained evaluations of the relationship between functional connectivity and ongoing cognition (Pedersen *et al* 2018), such as decision-making. In our present study, based on the identified flexible and robust architectures displayed in Fig. 4, the statistics of flexible and robust variability metrics were first completed (Fig. 5), which showed significant differences between the postgraduate students and junior high school students ($p < 0.05$). And when using the flexible and robust variability metrics to classify the two groups, an accuracy of 92.50% could be achieved (Fig. 6), while if only the raw coherence metrics were used, no satisfying results would be obtained, which further validated the capacity of the proposed protocols in capturing the fluctuating temporal variability in resting-state networks, as well as identifying distinct groups.

Quantitatively, small-worldness reflects regional specialization and information transfer efficiency of a given network, the *CC* and *LE* are the aggregation of the node and reflect the capacity for specialized processing of the local region; by contrast, the *CPL* and *GE* denote the functional integration of multiple brain regions, and all of these parameters can effectively evaluate the efficiency related to the specific information processing in the brain (Cozzo *et al* 2015). In this study, the temporal fuzzy entropy of these parameters (i.e., *CC*, *GE*, *LE*, *CPL*, and small-worldness) is thought to has the potential to quantitatively measure the local and global flexibility in the brain. As displayed in Figs. 7 to 10, what is interesting was the opposite decision-making behaviors between adolescents and adults under unfair conditions. In particular, in postgraduate students, we found the network variability parameters were negatively related to both AR and CW (Figs. 7 and 8), while the opposite relationships were found in junior high school students as these parameters were significantly positively related to individual AR and CW (Figs. 9 and 10). A small AR means an individual prefers fairness by rejecting the current unfair offer to punish the unfair behavior of the proposer (Yamagishi *et al* 2009), which thus leads to the lower task earning (i.e., smaller CW). In fact, the studies focusing on childhood development and socialization have primarily confirmed the increase of the preference for fairness from adolescence to adulthood (Marchetti *et al* 2019, Castelli *et al* 2014). Along with their growing up, the individuals' sociality increases and they are increasingly capable of using a multi-dimensional rule to deal with the current decision situation (van Duijvenvoorde *et al* 2010). Since this study was the first work to explore the potential relationships between resting-state brain network variability and individual decision behaviors, based on these considerations mentioned above, we believed that compared to those postgraduate students, junior high school students were more likely to accept the offer

given by the others, even those unfair ones, as they preferred current interests over fairness (Si *et al* 2020b). By contrast, the postgraduate students focused more on the intention and preferred the fairness (Peterburs *et al* 2017), if the unfairness occurs, they would like to reject the unfair offer in this situation. This might lead to a large AR in junior high school students but the high rejection rates in postgraduate students, as well as the opposite relationships between network variability and decision behaviors for both groups.

One possible limitation of this study would be that although sparse electrodes could reduce the effect of volume conduction on EEG and related networks, theoretically, EEG source localization could eliminate the volume conduction effect by projecting scalp EEG back to the cortex. In the future, by performing the EEG source localization, we will further investigate the fluctuating temporal variability of brain networks on the cortical layer, to further uncover the neural basis of network variability and its relationships with human cognition.

5. Conclusion

In summary, our present study first validated the capacity of fuzzy entropy in quantitatively measuring the fluctuating temporal patterns of the time-varying resting-state brain networks. When applying in the decision-making and P300 EEG datasets, the corresponding inherent fluctuating temporal patterns of resting-state networks were effectively captured; in particular, the flexible and robust architectures of the brain at rest were identified and distributed at the bilateral temporal lobe and frontal/occipital lobe, respectively. Moreover, the corresponding variability metrics not only helped differentiate different groups but also closely related to the individual decision behaviors, which could facilitate our knowledge of the human cognitive process, such as decision-making.

Acknowledgments

This work was supported by the National Natural Science Foundation of China (#61961160705, #U19A2082, #61901077), the Key Research and Development Program of Guangdong Province, China (#2018B030339001), the Science and Technology Development Fund, Macau SAR (File no. 0045/2019/AFJ), and the Project of Science and Technology Department of Sichuan Province (#2021YFSY0040, #2020ZYD013, #2018JZ0073).

Appendix

Conventional approaches

In essence, the variance (also the standard-deviation) , as a straightforward method, has been used to measure the uncertainty of a given signal (Dionisio *et al* 2007), which is usually in the resting-state fMRI studies (Hindriks *et al* 2016, Sakoglu *et al* 2010). In addition, Zalesky and colleagues also used the univariate test statistic to measure the time-varying correlation coefficient fluctuations for pairwise regions (Zalesky *et al* 2014). In this study, to first validate the benefits of the fuzzy entropy, these two traditional methods i.e., the variance and non-linear test statistic, were also used to estimate the corresponding temporal complexity of

the simulated network edges, and the corresponding performance of the fuzzy entropy was then statistically compared with that of the two traditional methods. Here, the corresponding definitions of both methods were further depicted below.

Concerning the variance, V, for each of the five network edges is formulized as follow;

$$V = \frac{1}{L-1}\sum_{i=1}^{L}(p_i - \mu)^2 \quad \text{(A1)}$$

where $p = p_1, p_2, \ldots, p_L$ denotes the time series of the simulated network edge, V denotes the variance of the time series, and μ denotes the mean of the signal.

For the non-linear test statistic, let m be the median of p and let $n_1, n_2, \ldots, n_J$ be the samples for which p crosses m. p then makes J-1 consecutive excursions from m. The length I_n and height H_n of the j-th excursion are defined as $I_n = n_{j+1} - n_j$ and $H_n = max\{|p_i - m| : n_j < i < n_{j+1}\}$, respectively. The non-linear test statistic (Zalesky *et al* 2014, Hindriks *et al* 2016) is finally defined as,

$$\chi = \sum_{j=1}^{J-1} \left| I_j^{\alpha} H_j^{\beta} \right| \quad \text{(A2)}$$

where α and β control the relative weighting of the length and height for each excursion. Meanwhile, following Zalesky and colleagues (Zalesky *et al* 2014), in this study, we then set $\alpha = 0.9$ and $\beta = 1$.

Validation on resting-state P300 EEG

Aiming to validate its applicability, the independent group of resting-state EEG datasets recorded before an oddball P300 task (Li *et al* 2019) was further analyzed by applying the same analytical protocols.

After being preprocessed with the same analytical protocols, 19 healthy right-handed participants (6 females, age range of 20-41 years, and mean 29.37 years) were included in the following analysis. They had the normal or corrected-to-normal visual acuity, and none of them had histories of substance abuse, took the medication with deleterious effects on cognition, and had a neurological illness.

Their resting-state EEG datasets were recorded using the Symtop amplifier (Symtop Instrument, Beijing, China) and a 16-channel Ag/AgCl electrode cap (BrainMaster, Inc., Shenzhen, China), whose electrodes (Fp1/2, F3/4, C3/C4, P3/4, O1/2, F7/8, T3/4/5/6) were positioned according to the 10-20 international electrode system. Electrode AFz served as the reference. The predefined sampling rate is 1,000 Hz and the online bandpass filtering is 0.05-100 Hz. The impedance per electrode was kept below 5 KΩ throughout the experiment.

Fig. A1 displays the network edges with the 20% largest (i.e., flexible, Fig. A1a) and 20% smallest (i.e., robust, Fig. A1b) fuzzy entropy, respectively, as well as the corresponding nodal degree distribution (Fig. A1c). Coincided with the findings of the postgraduate students and junior high school students in the UG task, the flexible architectures were also distributed at the bilateral temporal lobe (Fig. A1a), whose electrodes were printed with deep red color in Fig. A1c. Meanwhile, Fig. A1b further illustrates a robust DMN-like architecture, which linked the frontal and occipital lobe (i.e., the electrodes with deep blue color in Fig. A1c).

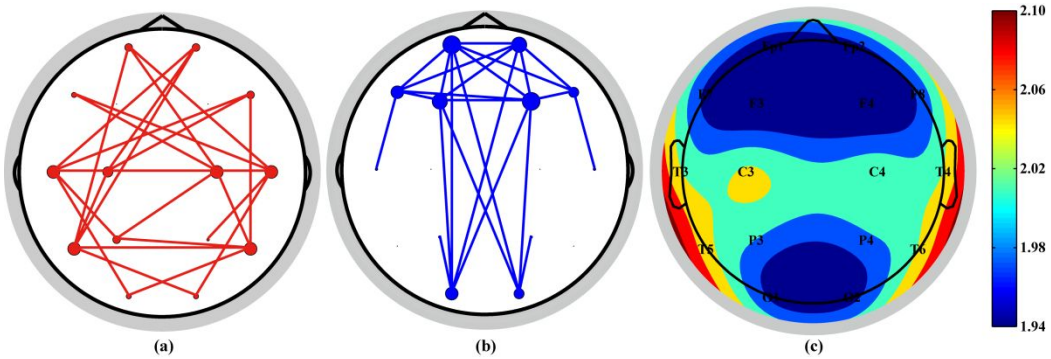

Fig. A1. Scalp topologies with the 20% largest and smallest fuzzy entropy for resting P300. (a) Flexible architecture, (b) Robust architecture, and (c) Nodal degree distribution. In subfigures (a, b), the size of each electrode is proportional to its binary degree in the 20% largest and smallest network, respectively.

References

Abasolo D, Hornero, R, Espino, P, Alvarez, D,Poza, J 2006 Entropy analysis of the EEG background activity in Alzheimer's disease patients *Physiol Meas* **27** 241-53.

Acharya U R, Fujita, H, Sudarshan, V K, Bhat, S,Koh, J E W 2015 Application of entropies for automated diagnosis of epilepsy using EEG signals: A review *Knowl-Based Syst* **88** 85-96.

Allen E A, Damaraju, E, Plis, S M, Erhardt, E B, Eichele, T,Calhoun, V D 2014 Tracking whole-brain connectivity dynamics in the resting state *Cereb Cortex* **24** 663-76.

Anticevic A, Cole, M W, Murray, J D, Corlett, P R, Wang, X J,Krystal, J H 2012 The role of default network deactivation in cognition and disease *Trends Cogn Sci* **16** 584-92.

Bassett D S,Bullmore, E T 2017 Small-World Brain Networks Revisited *Neuroscientist* **23** 499-516.

Betzel R F, Fukushima, M, He, Y, Zuo, X N,Sporns, O 2016 Dynamic fluctuations coincide with periods of high and low modularity in resting-state functional brain networks *NeuroImage* **127** 287-97.

Bledowski C, Prvulovic, D, Hoechstetter, K, Scherg, M, Wibral, M, Goebel, R,Linden, D E 2004 Localizing P300 generators in visual target and distractor processing: a combined event-related potential and functional magnetic resonance imaging study *J Neurosci* **24** 9353-60.

Braun U, Schafer, A, Walter, H, Erk, S, Romanczuk-Seiferth, N, Haddad, L, Schweiger, J I, Grimm, O, Heinz, A, Tost, H, Meyer-Lindenberg, A,Bassett, D S 2015 Dynamic reconfiguration of frontal brain networks during executive cognition in humans *Proc Natl Acad Sci USA* **112** 11678-83.

Buckner R L,Vincent, J L 2007 Unrest at rest: Default activity and spontaneous network correlations *NeuroImage* **37** 1091-6.

Cao Z, Lai, K L, Lin, C T, Chuang, C H, Chou, C C,Wang, S J 2018 Exploring resting-state EEG complexity before migraine attacks *Cephalalgia* **38** 1296-306.

Cao Z, Lin, C-T, Lai, K-L, Ko, L-W, King, J-T, Liao, K-K, Fuh, J-L,Wang, S-J 2020 Extraction of SSVEPs-Based Inherent Fuzzy Entropy Using a Wearable Headband EEG in Migraine Patients *IEEE Transactions on Fuzzy Systems* **28** 14-27.

Cao Z H,Lin, C T 2018 Inherent Fuzzy Entropy for the Improvement of EEG Complexity Evaluation *IEEE Trans Fuzzy Syst* **26** 1032-5.

Castelli I, Massaro, D, Sanfey, A G,Marchetti, A 2010 Fairness and intentionality in children's decision-making *Int Rev Econ* **57** 269-88.

Castelli I, Massaro, D, Sanfey, A G,Marchetti, A 2014 "What is fair for you?" Judgments and decisions about fairness and Theory of Mind *Eur J Dev Psychol* **11** 49-62.

Cecchetto C, Korb, S, Rumiati, R I,Aiello, M 2017 Emotional reactions in moral decision-making are influenced by empathy and alexithymia *Soc Neurosci-UK* 1-15.

Chen W, Wang, Z, Xie, H,Yu, W 2007 Characterization of surface EMG signal based on fuzzy entropy *IEEE Trans Neural Syst Rehabil Eng* **15** 266-72.

Chen W, Zhuang, J, Yu, W,Wang, Z 2009 Measuring complexity using FuzzyEn, ApEn, and SampEn *Med Eng Phys* **31** 61-8.

Cozzo E, Kivela, M, De Domenico, M, Sole-Ribalta, A, Arenas, A, Gomez, S, Porter, M A,Moreno, Y 2015 Structure of triadic relations in multiplex networks *New J Phys* **17**.

Damoiseaux J, Rombouts, S, Barkhof, F, Scheltens, P, Stam, C, Smith, S M,Beckmann, C 2006 Consistent resting-state networks across healthy subjects *Proc Natl Acad Sci USA* **103** 13848-53.

Dimitrakopoulos G N, Kakkos, I, Dai, Z, Wang, H, Sgarbas, K, Thakor, N, Bezerianos, A,Sun, Y 2018 Functional Connectivity Analysis of Mental Fatigue Reveals Different Network Topological Alterations Between Driving and Vigilance Tasks *IEEE Trans Neural Syst Rehabil Eng* **26** 740-9.

Dionisio A, Menezes, R,Mendes, D A 2007 Entropy and uncertainty analysis in financial markets *arXiv preprint*.

Dong L, Li, F, Liu, Q, Wen, X, Lai, Y, Xu, P,Yao, D 2017 MATLAB Toolboxes for Reference Electrode Standardization Technique (REST) of Scalp EEG *Front Neurosci* **11** 601.

Falahpour M, Chang, C, Wong, C W,Liu, T T 2018 Template-based prediction of vigilance fluctuations in resting-state fMRI *NeuroImage* **174** 317-27.

Fox P T, Burton, H,Raichle, M E 1987 Mapping human somatosensory cortex with positron emission tomography *J Neurosurg* **67** 34-43.

Gao J B, Hu, J, Liu, F Y,Cao, Y H 2015 Multiscale entropy analysis of biological signals: a fundamental bi-scaling law *Front Comput Neurosci* **9**.

Garrett D D, Kovacevic, N, Mcintosh, A R,Grady, C L 2011 The Importance of Being Variable *J Neurosci* **31** 4496-503.

Gladwin T E, Figner, B, Crone, E A,Wiers, R W 2011 Addiction, adolescence, and the integration of control and motivation *Dev Cogn Neurosci* **1** 364-76.

Guroglu B, Van Den Bos, W,Crone, E A 2009 Fairness considerations: increasing understanding of intentionality during adolescence *J Exp Child Psychol* **104** 398-409.

He T, Clifford, G,Tarassenko, L 2005 Application of independent component analysis in removing artefacts from the electrocardiogram *Neural Computing and Applications* **15** 105-16.

Hearne L J, Cocchi, L, Zalesky, A,Mattingley, J B 2017 Reconfiguration of Brain Network Architectures between Resting-State and Complexity-Dependent Cognitive Reasoning *Journal of Neuroscience* **37** 8399-411.

Hindriks R, Adhikari, M H, Murayama, Y, Ganzetti, M, Mantini, D, Logothetis, N K,Deco, G 2016 Can sliding-window correlations reveal dynamic functional connectivity in resting-state fMRI? *NeuroImage* **127** 242-56.

Hoffmann R,Tee, J-Y 2006 Adolescent–adult interactions and culture in the ultimatum game *J Econ Psychol* **27** 98-116.

Huang Y, Zhang, J, Cui, Y, Yang, G, He, L, Liu, Q,Yin, G 2017 How Different EEG References Influence Sensor Level Functional Connectivity Graphs *Front Neurosci* **11** 368.

Huerta M F,Kaas, J H 1990 Supplementary Eye Field as Defined by Intracortical Microstimulation - Connections in Macaques *J Comp Neurol* **293** 299-330.

Hutchison R M, Womelsdorf, T, Allen, E A, Bandettini, P A, Calhoun, V D, Corbetta, M, Della Penna, S, Duyn, J H, Glover, G H, Gonzalez-Castillo, J, Handwerker, D A, Keilholz, S, Kiviniemi, V, Leopold, D A, De Pasquale, F, Sporns, O, Walter, M,Chang, C 2013 Dynamic functional connectivity: promise, issues, and interpretations *NeuroImage* **80** 360-78.

Jann K, Dierks, T, Boesch, C, Kottlow, M, Strik, W,Koenig, T 2009 BOLD correlates of EEG alpha phase-locking and the fMRI default mode network *NeuroImage* **45** 903-16.

Jiang Y, Tian, Y,Wang, Z 2019 Causal Interactions in Human Amygdala Cortical Networks across the Lifespan *Sci Rep* **9** 5927.

Kim B M, Lee, J, Choi, A R, Chung, S J, Park, M, Koo, J W, Kang, U G,Choi, J S 2021 Event-related brain response to visual cues in individuals with Internet gaming disorder: relevance to attentional bias and decision-making *Transl Psychiatry* **11** 258.

Li F, Liu, T, Wang, F, Li, H, Gong, D, Zhang, R, Jiang, Y, Tian, Y, Guo, D,Yao, D 2015 Relationships between the resting-state network and the P3: Evidence from a scalp EEG study *Sci Rep* **5** 15129.

Li F, Tao, Q, Peng, W, Zhang, T, Si, Y, Zhang, Y, Yi, C, Biswal, B, Yao, D,Xu, P 2020 Inter-subject P300 variability relates to the efficiency of brain networks reconfigured from resting-to task-state: Evidence from a simultaneous event-related EEG-fMRI study *NeuroImage* **205** 116285.

Li F, Wang, J, Liao, Y, Yi, C, Jiang, Y, Si, Y, Peng, W, Yao, D, Zhang, Y, Dong, W,Xu, P 2019 Differentiation of Schizophrenia by Combining the Spatial EEG Brain Network Patterns of Rest and Task P300 *IEEE Trans Neural Syst Rehabil Eng* **27** 594-602.

Li N, Ma, N, Liu, Y, He, X S, Sun, D L, Fu, X M, Zhang, X C, Han, S H,Zhang, D R 2013a Resting-State Functional Connectivity Predicts Impulsivity in Economic Decision-Making *J Neurosci* **33** 4886-95.

Li P, Liu, C, Wang, X, Li, B, Che, W,Liu, C 2013b. Cross-Sample Entropy and Cross-Fuzzy Entropy for Testing Pattern Synchrony: How Results Vary with Different Threshold Value r. *World Congress on Medical Physics and Biomedical Engineering May 26-31, 2012, Beijing, China.*

Li Y, Pan, J, Wang, F,Yu, Z 2013c A hybrid BCI system combining P300 and SSVEP and its application to wheelchair control *IEEE Trans Biomed Eng* **60** 3156-66.

Long J, Li, Y, Wang, H, Yu, T, Pan, J,Li, F 2012 A hybrid brain computer interface to control the direction and speed of a simulated or real wheelchair *IEEE Trans Neural Syst Rehab Eng* **20** 720-9.

Lurie D, Kessler, D, Bassett, D, Betzel, R F, Breakspear, M, Keilholz, S, Kucyi, A, Liégeois, R, Lindquist, M A,Mcintosh, A R 2018 On the nature of resting fMRI and time-varying functional connectivity.

Mantini D, Perrucci, M G, Del Gratta, C, Romani, G L,Corbetta, M 2007 Electrophysiological signatures of resting state networks in the human brain *Proc Natl Acad Sci USA* **104** 13170-5.

Marchetti A, Baglio, F, Castelli, I, Griffanti, L, Nemni, R, Rossetto, F, Valle, A, Zanette, M,Massaro, D 2019 Social Decision Making in Adolescents and Young Adults: Evidence From the Ultimatum Game and Cognitive Biases *Psychol Rep* **122** 135-54.

Marx E, Deutschlander, A, Stephan, T, Dieterich, M, Wiesmann, M,Brandt, T 2004 Eyes open and eyes closed as rest conditions: impact on brain activation patterns *NeuroImage* **21** 1818-24.

Marx E, Stephan, T, Nolte, A, Deutschlander, A, Seelos, K C, Dieterich, M,Brandt, T 2003 Eye closure in darkness animates sensory systems *NeuroImage* **19** 924-34.

Masulli P, Masulli, F, Rovetta, S, Lintas, A,Villa, A E P 2020 Fuzzy Clustering for Exploratory Analysis of EEG Event-Related Potentials *IEEE Transactions on Fuzzy Systems* **28** 28-38.

Moon S E, Chen, C J, Hsieh, C J, Wang, J L,Lee, J S 2020 Emotional EEG classification using connectivity features and convolutional neural networks *Neural Networks* **132** 96-107.

Northoff G, Qin, P M,Nakao, T 2010 Rest-stimulus interaction in the brain: a review *Trends Neurosci* **33** 277-84.

Pedersen M, Zalesky, A, Omidvarnia, A,Jackson, G D 2018 Multilayer network switching rate predicts brain performance *Proc Natl Acad Sci USA* **115** 13376-81.

Pena-Gomez C, Avena-Koenigsberger, A, Sepulcre, J,Sporns, O 2018 Spatiotemporal Network Markers of Individual Variability in the Human Functional Connectome *Cereb Cortex* **28** 2922-34.

Peterburs J, Voegler, R, Liepelt, R, Schulze, A, Wilhelm, S, Ocklenburg, S,Straube, T 2017 Processing of fair and unfair offers in the ultimatum game under social observation *Sci Rep* **7** 44062.

Pincus S 1995 Approximate Entropy (Apen) as a Complexity Measure *Chaos* **5** 110-7.

Pincus S M 1991 Approximate Entropy as a Measure of System-Complexity *Proc Natl Acad Sci USA* **88** 2297-301.

Pincus S M,Goldberger, A L 1994 Physiological time-series analysis: what does regularity quantify? *Am J Physiol* **266** H1643-56.

Polich J 2007 Updating P300: an integrative theory of P3a and P3b *Clin Neurophysiol* **118** 2128-48.

Prestel M, Steinfath, T P, Tremmel, M, Stark, R,Ott, U 2018 fMRI BOLD Correlates of EEG Independent Components: Spatial Correspondence With the Default Mode Network *Front Hum Neurosci* **12**.

Preuss N, Brändle, L S, Hager, O M, Haynes, M, Fischbacher, U,Hasler, G 2016 Inconsistency and social decision making in patients with Borderline Personality Disorder *Psychiat Res* **243** 115-22.

Qin Y, Xu, P,Yao, D 2010 A comparative study of different references for EEG default mode

network: the use of the infinity reference *Clin Neurophysiol* **121** 1981-91.

Rubia K, Overmeyer, S, Taylor, E, Brammer, M, Williams, S C R, Simmons, A, Andrew, C,Bullmore, E T 2000 Functional frontalisation with age: mapping neurodevelopmental trajectories with fMRI *Neurosci Biobehav Rev* **24** 13-9.

Rubinov M,Sporns, O 2010 Complex network measures of brain connectivity: uses and interpretations *NeuroImage* **52** 1059-69.

Sakoglu U, Pearlson, G D, Kiehl, K A, Wang, Y M, Michael, A M,Calhoun, V D 2010 A method for evaluating dynamic functional network connectivity and task-modulation: application to schizophrenia *Magn Reson Mater Phy* **23** 351-66.

Shen H H 2015 Core Concept: Resting-state connectivity *Proc Natl Acad Sci USA* **112** 14115-6.

Shirer W R, Ryali, S, Rykhlevskaia, E, Menon, V,Greicius, M D 2012 Decoding subject-driven cognitive states with whole-brain connectivity patterns *Cereb Cortex* **22** 158-65.

Si Y, Jiang, L, Tao, Q, Chen, C, Li, F, Jiang, Y, Zhang, T, Cao, X, Wan, F, Yao, D,Xu, P 2019a Predicting individual decision-making responses based on the functional connectivity of resting-state EEG *J Neural Eng* **16** 066025.

Si Y, Li, F, Duan, K, Tao, Q, Li, C, Cao, Z, Zhang, Y, Biswal, B, Li, P, Yao, D,Xu, P 2020a Predicting individual decision-making responses based on single-trial EEG *NeuroImage* **206** 116333.

Si Y, Li, F, Li, F, Tu, J, Yi, C, Tao, Q, Zhang, X, Pei, C, Gao, S, Yao, D,Xu, P 2020b The Growing from Adolescence to Adulthood Influences the Decision Strategy to Unfair Situations *IEEE Trans Cogn Dev Syst* 1-.

Si Y, Wu, X, Li, F, Zhang, L, Duan, K, Li, P, Song, L, Jiang, Y, Zhang, T, Zhang, Y, Chen, J, Gao, S, Biswal, B, Yao, D,Xu, P 2019b Different Decision-Making Responses Occupy Different Brain Networks for Information Processing: A Study Based on EEG and TMS *Cereb Cortex* **29** 4119-29.

Simons S, Espino, P,Abásolo, D 2018 Fuzzy Entropy Analysis of the Electroencephalogram in Patients with Alzheimer's Disease: Is the Method Superior to Sample Entropy? *Entropy* **20**.

Sun J, Liu, Z, Rolls, E T, Chen, Q, Yao, Y, Yang, W, Wei, D, Zhang, Q, Zhang, J, Feng, J,Qiu, J 2019 Verbal Creativity Correlates with the Temporal Variability of Brain Networks During the Resting State *Cereb Cortex* **29** 1047-58.

Sutter M 2007 Outcomes versus intentions: On the nature of fair behavior and its development with age *J Econ Psychol* **28** 69-78.

Takahashi T, Cho, R Y, Mizuno, T, Kikuchi, M, Murata, T, Takahashi, K,Wada, Y 2010 Antipsychotics reverse abnormal EEG complexity in drug-naive schizophrenia: A multiscale entropy analysis *NeuroImage* **51** 173-82.

Thompson W H, Brantefors, P,Fransson, P 2017 From static to temporal network theory: Applications to functional brain connectivity *Netw Neurosci* **1** 69-99.

Tian Y, Yang, L, Chen, S F, Guo, D Q, Ding, Z C, Tam, K Y,Yao, D Z 2017a Causal interactions in resting-state networks predict perceived loneliness *Plos One* **12**.

Tian Y, Zhang, H, Jiang, Y, Li, P,Li, Y 2019 A Fusion Feature for Enhancing the Performance of Classification in Working Memory Load With Single-Trial Detection

IEEE Trans Neural Syst Rehabil Eng **27** 1985-93.

Tian Y, Zhang, H, Xu, W, Zhang, H, Yang, L, Zheng, S,Shi, Y 2017b Spectral Entropy Can Predict Changes of Working Memory Performance Reduced by Short-Time Training in the Delayed-Match-to-Sample Task *Front Hum Neurosci* **11** 437.

Turetsky B I, Dress, E M, Braff, D L, Calkins, M E, Green, M F, Greenwood, T A, Gur, R E, Gur, R C, Lazzeroni, L C,Nuechterlein, K H 2015 The utility of P300 as a schizophrenia endophenotype and predictive biomarker: clinical and socio-demographic modulators in COGS-2 *Schizophr Res* **163** 53-62.

Van Duijvenvoorde A C, Jansen, B R, Visser, I,Huizenga, H M 2010 Affective and cognitive decision-making in adolescents *Dev Neuropsychol* **35** 539-54.

Villafaina S, Collado-Mateo, D, Cano-Plasencia, R, Gusi, N,Fuentes, J P 2019 Electroencephalographic response of chess players in decision-making processes under time pressure *Physiol Behav* **198** 140-3.

Wang H, Xu, G, Wang, X, Sun, C, Zhu, B, Fan, M, Jia, J, Guo, X,Sun, L 2019 The reorganization of resting-state brain networks associated with motor imagery training in chronic stroke patients *IEEE Trans Neural Syst Rehabil Eng*.

Wang L, Zheng, J, Huang, S,Sun, H 2015a P300 and Decision Making under Risk and Ambiguity *Comput Intell Neurosci* **2015** 108417.

Wang X H, Li, L H, Xu, T,Ding, Z X 2015b Investigating the Temporal Patterns within and between Intrinsic Connectivity Networks under Eyes-Open and Eyes-Closed Resting States: A Dynamical Functional Connectivity Study Based on Phase Synchronization *Plos One* **10**.

Wang Y, Zhang, Z, Bai, L, Lin, C, Osinsky, R,Hewig, J 2017 Ingroup/outgroup membership modulates fairness consideration: neural signatures from ERPs and EEG oscillations *Sci Rep* **7** 39827.

Xiang J, Li, C G, Li, H F, Cao, R, Wang, B, Han, X H,Chen, J J 2015 The detection of epileptic seizure signals based on fuzzy entropy *J Neurosci Methods* **243** 18-25.

Xie H B, Zheng, Y P, Guo, J Y,Chen, X 2010 Cross-fuzzy entropy: A new method to test pattern synchrony of bivariate time series *Information Sciences* **180** 1715-24.

Yamagishi T, Horita, Y, Takagishi, H, Shinada, M, Tanida, S,Cook, K S 2009 The private rejection of unfair offers and emotional commitment *Proc Natl Acad Sci USA* **106** 11520-3.

Yang A C, Hong, C J, Liou, Y J, Huang, K L, Huang, C C, Liu, M E, Lo, M T, Huang, N E, Peng, C K, Lin, C P,Tsai, S J 2015 Decreased Resting-State Brain Activity Complexity in Schizophrenia Characterized by Both Increased Regularity and Randomness *Hum Brain Mapp* **36** 2174-86.

Yao D 2001 A method to standardize a reference of scalp EEG recordings to a point at infinity *Physiol Meas* **22** 693.

Yu H, Lei, X, Song, Z, Liu, C,Wang, J 2020 Supervised Network-Based Fuzzy Learning of EEG Signals for Alzheimer's Disease Identification *IEEE Trans Fuzzy Syst* **28** 60-71.

Yu H, Wu, X, Cai, L, Deng, B,Wang, J 2018 Modulation of Spectral Power and Functional Connectivity in Human Brain by Acupuncture Stimulation *IEEE Trans Neural Syst Rehabil Eng* **26** 977-86.

Yu Q, Erhardt, E B, Sui, J, Du, Y, He, H, Hjelm, D, Cetin, M S, Rachakonda, S, Miller, R L,

Pearlson, G,Calhoun, V D 2015 Assessing dynamic brain graphs of time-varying connectivity in fMRI data: application to healthy controls and patients with schizophrenia *NeuroImage* **107** 345-55.

Zalesky A, Fornito, A, Cocchi, L, Gollo, L L,Breakspear, M 2014 Time-resolved resting-state brain networks *Proc Natl Acad Sci USA* **111** 10341-6.

Zeng L, Shen, H, Liu, L, Wang, L, Li, B, Fang, P, Zhou, Z, Li, Y,Hu, D 2012 Identifying major depression using whole-brain functional connectivity: a multivariate pattern analysis *Brain* **135** 1498-507.

Zhang R, Yao, D, Valdés-Sosa, P A, Li, F, Li, P, Zhang, T, Ma, T, Li, Y,Xu, P 2015 Efficient resting-state EEG network facilitates motor imagery performance *J Neural Eng* **12** 066024.

Zhou G, Liu, P, He, J, Dong, M, Yang, X, Hou, B, Von Deneen, K, Qin, W,Tian, J 2012 Interindividual reaction time variability is related to resting-state network topology: an electroencephalogram study *Neuroscience* **202** 276-82.